The duration of mitosis and daughter cell size are modulated by nutrients in budding yeast

Ricardo M. Leitao[1], Annie Pham[1,2], Douglas R. Kellogg[1,3]

[1] Department of Molecular, Cell and Developmental Biology, University of California, 1156 High Street, Santa Cruz, CA 95064, USA

[2] Department of Craniofacial Biology, Denver Anschütz Medical Campus, University of Colorado, 12801 E. 17th Ave, Aurora, CO 80045, USA

[3] Corresponding Author: dkellogg@ucsc.edu. Phone: 831 459 5659.

Running Title: Control of cell growth and size in mitosis

Manuscript length: 34,017 characters

Abstract

Previous studies have suggested that the size of budding yeast cells is controlled almost entirely by a cell size checkpoint that acts in G1 phase. In contrast, we show here that a previously unknown checkpoint that acts during mitosis plays a major role in cell size control. Over 80% of cell growth in rich nutrient sources occurs during mitosis, while only 8% occurs during G1 phase. When growth is slowed by poor nutrients, the mitotic checkpoint compensates by prolonging both metaphase and anaphase, thereby increasing the duration of growth. The mitotic delay in poor nutrients is controlled partly by inhibitory phosphorylation of Cdk1 and partly by a novel mechanism that is independent of Cdk1 inhibitory phosphorylation. PP2A associated with the conserved Rts1 regulatory subunit is a key component of the checkpoint and appears to control cell size by enforcing a mechanistic link between growth rate and size.

Introduction

Cell growth during the cell cycle must be precisely controlled to ensure that cell division yields two viable cells of a defined size. This is achieved by cell size checkpoints, which delay key cell cycle transitions until an appropriate amount of growth has occurred. The mechanisms by which cell size checkpoints measure growth and trigger cell cycle transitions are poorly understood.

An interesting feature of cell size checkpoints is that they can be modulated by nutrients. Thus, in many kinds of cells the amount of growth required to proceed through the cell cycle is reduced in poor nutrients, which can lead to a nearly 2-fold reduction in size (Young and Fantes, 1987; Fantes and Nurse, 1977; Kimball and Vogt-Köhne, 1961; Weisz, 1954; Johnston et al., 1977). Nutrient modulation of cell size is likely an adaptive response that allows cells to maximize the number of cell divisions that can occur when nutrients are limiting. Nutrient modulation of cell size is of interest because it likely works by modulating the threshold amount of growth required for cell cycle progression. Thus, discovering mechanisms of nutrient modulation of cell size should lead to broadly relevant insight into how cell size is controlled.

Cell size checkpoints are best understood in yeast, where two checkpoints have been defined. One operates at cell cycle entry in G1 phase, while the other operates at mitotic entry (Hartwell and Unger, 1977; Harvey et al., 2005; Nurse, 1975). The G1 phase checkpoint delays transcription of G1 cyclins, which is thought to be the critical event that marks commitment to enter the cell cycle (Cross, 1988; Nash et al., 1988). The mitotic checkpoint delays mitosis via the Wee1 kinase, which phosphorylates and inhibits mitotic Cdk1 (Nurse, 1975; Gould and Nurse, 1989).

In budding yeast, several lines of evidence suggest that cell size control occurs almost entirely at the G1 checkpoint. Budding yeast cell division is asymmetric, yielding a large mother cell and a small daughter cell. The small daughter cell spends more time undergoing cell growth in G1 prior to cell cycle entry (Hartwell and Unger, 1977; Johnston et al., 1977). This observation led to the initial idea of a G1 cell size checkpoint that blocks cell cycle entry until sufficient growth has occurred. The checkpoint is thought to control G1 cyclin transcription because loss of *CLN3*, the key early G1 cyclin that drives cell cycle entry, causes a delay in G1 phase (Richardson et al., 1989; Cross, 1990). Cell growth continues during the delay, leading to abnormally large cells (Cross, 1988). Conversely, overexpression of *CLN3* causes cell cycle entry at a reduced cell size (Cross, 1988; Nash et al., 1988). In contrast, loss of the Wee1 kinase, a key component of the mitotic checkpoint, causes only mild cell size defects in budding yeast (Jorgensen et al., 2002; Harvey et al., 2005; Harvey and Kellogg, 2003). Together, these observations have suggested that cell size control occurs primarily during G1, and that Cln3 is a critical regulator of cell size that links cell cycle entry to cell growth.

Although significant cell size control occurs in G1 phase, there is evidence that important size control occurs at other phases in the cell cycle in budding yeast. For example, cells lacking all known regulators of the G1 cell size checkpoint show robust nutrient modulation of cell size (Jorgensen et al., 2004). This could be explained by the existence of additional G1 cell size control mechanisms that have yet to be discovered, but it could also suggest that normal nutrient modulation of cell size requires checkpoints that work outside of G1 phase. More evidence comes from the observation that daughter cells complete mitosis at a significantly smaller size in poor nutrients than in rich nutrients (Johnston et al., 1977). This suggests the existence of a checkpoint that operates after G1, during bud growth, to control the size at which daughter cells are born. This possibility has not received significant attention because early work suggested that the duration of daughter bud growth is invariant and independent of nutrients (Hartwell and Unger, 1977). As a result, it has been thought that birth of small daughter cells in poor nutrients is a simple consequence of their reduced growth rate, rather than active size control. However, this has not been tested by directly measuring the duration of

daughter cell growth in rich and poor nutrients, so it remains possible that checkpoints actively modulate the extent of daughter cell growth to control cell size at completion of mitosis.

Further evidence for size control outside of G1 phase has come from analysis of nutrient modulation of cell size. Protein phosphatase 2A associated with the Rts1 regulatory subunit ($PP2A^{Rts1}$) is required for nutrient modulation of cell size (Artiles et al., 2009). Proteome-wide analysis of targets of $PP2A^{Rts1}$ revealed that it controls critical components of both the G1 and mitotic cell size checkpoints, as well as several additional key regulators of mitotic progression (Zapata et al., 2014). The fact that $PP2A^{Rts1}$ is required for nutrient modulation of cell size, while regulators of the G1 checkpoint are not, could be explained by a model in which $PP2A^{Rts1}$ controls mitotic cell size checkpoints that play an important role in nutrient modulation of cell size.

Here, we set out to determine whether nutrient modulation of cell size occurs solely at the G1 checkpoint, or whether it occurs at other times during the cell cycle. To do this, we investigated how nutrients affect cell growth, cell size and cell cycle progression after G1 phase.

Results

The duration of mitosis is modulated by nutrients

Previous work suggested that the cell cycle events that occur after bud emergence have a constant duration that is independent of the growth rate set by nutrients (Hartwell and Unger, 1977). However, the limited tools available at the time meant that the duration of cell cycle events had to be inferred from indirect measurements. To more directly address this question, we first grew cells in a rich carbon source (2% dextrose) or a poor carbon source (2% glycerol + 2% ethanol) and determined the duration of mitosis by assaying levels of the mitotic cyclin Clb2 in synchronized cells. Clb2 persisted for a longer interval in cells growing in poor nutrients, which suggested that the duration of mitosis is increased (**Figure 1A**).

We next asked whether cells already in mitosis were sensitive to a shift from rich to poor carbon. Cells growing in rich carbon were synchronized and shifted to poor carbon when Clb2 reached peak levels and most cells had short mitotic spindles, indicating that they were in metaphase. A shift to poor carbon at this point in mitosis caused a prolonged metaphase delay, as well as delayed destruction of Clb2 (**Figures 1B,C**). In contrast, if cells were switched to poor carbon slightly later in mitosis, when cells were in anaphase, there was no delay in destruction of Clb2 or in completion of anaphase (**Figures 1D,E**). The insensitivity of anaphase cells to carbon source suggests that the metaphase delay is not due simply to a starvation response.

To further investigate the effects of nutrients, we used a combination of fluorescence and bright field microscopy to simultaneously monitor daughter bud growth and mitotic events in living cells. Bud growth was monitored by plotting daughter bud volume as a function of time. The duration of mitotic events was monitored by marking mitotic spindle poles with Spc42-GFP and plotting the distance between poles as a function of time. Initiation of metaphase corresponds to the initial separation of spindle poles, while the duration of metaphase corresponds to the interval when spindle poles remain separated by 1-2 microns within the mother cell (Winey and O'Toole, 2001; Lianga et al., 2013). Initiation of anaphase is detected when spindle poles begin to move further apart and one pole migrates into the daughter cell. We defined the duration of anaphase as the interval between anaphase initiation and the time when the spindle poles reached their maximum distance apart. GFP-tagged myosin was used to detect completion of cytokinesis, which is marked by disappearance of the myosin ring (Lippincott and Li, 1998). In addition to the stages of mitosis, we defined an S/G2 interval as the time from bud emergence to spindle pole separation, and G1 phase as the time from when the daughter cell completes cytokinesis to the time that it initiates formation of a new daughter bud.

Daughter cell growth was monitored for one complete bud growth cycle, from the time the bud emerged from the mother cell to the time that it initiated formation of a new bud at the end of the next G1 phase. Representative data for a cell growing in rich carbon are shown in **Figure 2A**, and data for a cell growing in poor carbon in **Figure 2B**. Examples of cell images taken during the course of bud growth are shown in **Figure 2C**. At least 25 cells were analyzed under each condition (See **Figure S1** for individual growth curves).

Growth of the daughter bud occurred throughout mitosis (**Figure 2**). To focus on the effects of carbon source on the duration of mitosis, we first plotted the average duration of each stage of mitosis for cells growing in rich or poor carbon (**Figure 3A**; see **Figure S2A** for scatter plots and p-values**)**. The durations of both metaphase and anaphase were significantly increased in poor carbon, although the greatest increase was observed for metaphase. The overall duration of mitosis, from the beginning of metaphase to cytokinesis was 52 minutes in rich carbon, and 68 minutes in poor carbon.

The durations of all cell cycle stages comprising a complete bud growth cycle in rich and poor carbon are shown in **Figure 3B (**see **Figure S2A** for scatter plots and p-values**)**. This

revealed that the fraction of the growth cycle that occurs in G1 phase increased in poor carbon, as previously reported (Hartwell and Unger, 1977).

Daughter cells complete mitosis at a smaller size in poor nutrients

We next plotted bud size at completion of each cell cycle stage (**Figure 3C;** see **Figure S2B** for scatter plots and p values). Metaphase was initiated at the same daughter cell size in both carbon sources (7 fL). Cells in poor carbon, however, completed each stage of mitosis at a significantly smaller size. Overall, cells in rich carbon completed cytokinesis at a volume of 57 fL, whereas cells in poor carbon completed mitosis at a volume of 35 fL. Cells in rich carbon underwent the same amount of growth in metaphase as in anaphase (25 fL vs 24 fL), while cells in poor carbon grew more in metaphase than in anaphase (16 fL vs 10fL).

Together, the data indicate that the duration of both metaphase and anaphase is increased in poor carbon, while daughter cell size at each mitotic transition is reduced. Thus, the data are inconsistent with a model in which cells complete mitosis at a reduced size in poor nutrients simply because their growth rate is reduced, while the duration of mitotic events is unchanged. Rather, the duration of mitosis and cell size at completion of mitosis are modulated in response to changes in carbon source that cause large changes in growth rate.

Most cell growth occurs during mitosis

Analysis of the data in **Figure 3C** shows that most growth occurs during mitosis**.** Thus, in rich carbon, 80% of the volume of a daughter cell is achieved during mitosis; growth of the daughter cell during the subsequent G1 adds only 5 fL, or 8% of the final volume of the daughter cell before it becomes a mother cell. In poor carbon, these numbers are shifted: 61% of the volume of a cell growing in poor carbon is achieved during mitosis; growth during the subsequent G1 adds 10 fL, or 23% of the final volume. Fission yeast cells show a similar expansion of G1 phase when grown in poor nitrogen (Costello et al., 1986; Su et al., 1996).

Growth rate changes during the cell cycle and is modulated by nutrients

The growth curves in **Figure 2** suggest that the growth cycle is comprised of distinct phases characterized by different growth rates. Previous studies suggested that growth rate changes during the cell cycle, but did not include analysis of growth during specific stages of mitosis in unperturbed single cells (Mitchison, 1958; Goranov et al., 2009; Ferrezuelo et al., 2012). To extend these studies, we calculated growth rates at each stage of the cell cycle in rich and poor carbon (**Figures 4 A,B**). When the bud first emerges, growth is relatively slow. Entry into mitosis initiates a fast growing phase that lasts nearly the entire length of mitosis. As cells complete anaphase the growth rate slows. A slow rate of growth persists during G1 phase. Poor carbon reduced the rate of growth in mitosis by half, but caused significantly smaller reductions in growth rate during other stages of the growth cycle.

Previous work found that the bud initially grows in a polar manner, and that activation of mitotic Cdk1 triggers a switch to isotropic growth that occurs over the entire surface of the bud (Farkaš et al., 1974; Lew and Reed, 1993; Barral et al., 1995; McCusker et al., 2007). Thus, the data indicate that the polar and isotropic growth phases occur at significantly different rates.

The effects of carbon source on daughter cell size are not due solely to changes in mother cell size

Mother cell size influences daughter cell size: small mothers produce small daughters, and large mothers produce large daughters (Johnston et al., 1977; Schmoller et al., 2015). In addition, newborn daughter cells progress through the G1 cell size checkpoint at a smaller size in poor carbon, which means that they initiate bud emergence and become mother cells at a smaller size (Johnston et al., 1979; Lorincz and Carter, 1979; Jorgensen and Tyers, 2004). Thus, we considered the possibility that reduced daughter cell size in poor carbon is primarily a

consequence of the reduced size of their mothers. In this model, mother cells become small in poor carbon because they pass the G1 cell size checkpoint at a reduced cell size, and they produce small daughters because they have a reduced biosynthetic capacity. This model does not explain the increased duration of mitosis in poor carbon, which suggests that decreased mother cell size is unlikely to be the sole factor influencing the size of daughter cells. Nevertheless, we analyzed the effects of mother cell size on daughter cell size and growth rate both within and between media conditions.

Growth rate was positively correlated with mother cell size in both rich and poor carbon (**Figure 5A**). Thus, daughters of large mothers grew faster than daughters of small mothers, consistent with the idea that mother cell size influences biosynthetic capacity. However, carbon source had a stronger influence on growth rate than mother cell size. This can be seen by the fact that mothers of similar size in rich and poor carbon had significantly different growth rates, which was true across the entire range of mother cell sizes (**Figure 5A**).

We also plotted daughter cell size at completion of cytokinesis versus mother cell size (**Figure 5B**). Daughter cell size was positively correlated with mother cell size in both conditions. Again, however, the influence of carbon source was much stronger. Mother cells growing in poor carbon that were the same size as mother cells in rich carbon consistently produced much smaller daughter cells. Thus, the reduced size at which daughter cells complete mitosis in poor carbon cannot be explained simply by reduced mother cell size.

Cell size at completion of mitosis is correlated with growth rate during mitosis

Previous studies found that cell size at the end of G1 phase is correlated with growth rate during G1 phase (Ferrezuelo et al., 2012; Johnston et al., 1979). The correlation held true when comparing cells growing in the same carbon source and when comparing cells growing in different carbon sources. To determine whether a similar relationship exists for growth during mitosis, we plotted daughter cell size at cytokinesis as a function of daughter bud growth rate during mitosis for cells growing in rich or poor carbon (**Figure 6**). Daughter cell size was strongly correlated with growth rate under both conditions.

$PP2A^{Rts1}$ is required for normal control of mitotic duration and cell size at completion of mitosis

We next searched for signals that modulate the duration of mitosis and daughter cell size in response to nutrients. In previous work, we discovered that *rts1*Δ cells show a nearly complete failure in nutrient modulation of cell size, which suggested that $PP2A^{Rts1}$ plays an important role (Artiles et al., 2009). We therefore tested the effects of a loss of function of Rts1 on mitotic duration and daughter cell size. Interpretation of results from *rts1*Δ cells would be complicated by the possibility that effects on bud growth and size could be a secondary consequence of pre-existing defects in mother cell size arising in previous generations. Therefore, we created an auxin-inducible degron version of Rts1 (*rts1-AID*), which allowed us to observe the immediate effects of inactivating $PP2A^{Rts1}$ (Nishimura et al., 2009). In the absence of auxin, *rts1-AID* did not cause significant defects in cell size or cell cycle progression **(Figures S3A,B)**. Addition of auxin caused rapid destruction of rts1-AID protein within 15-30 minutes (**Figure S3C**). Approximately 10% of the rts1-AID protein remained in the presence of auxin, and *rts1-AID* cells formed colonies more rapidly than *rts1*Δ cells at elevated temperatures (**Figure S3D**). Together, these observations suggest that *rts1-AID* causes a partial loss of function. Nevertheless, we utilized *rts1-AID* because it allowed analysis of bud growth and mitotic duration without the complication of aberrant mother cell size.

rts1-AID cells were released from a G1 arrest and auxin was added shortly before bud emergence. Destruction of rts1-AID caused an approximately 3-fold increase in the average duration of metaphase in both rich and poor carbon (**Figures 7A,B;** see **Figures S4A,B** for dot plots and p-values). The duration of anaphase was also increased, although not to the same

extent. Destruction of rts1-AID caused a large increase in the variance of metaphase duration compared to wild type cells (See dot plots in **Figure S4A,B**). Moreover, although the duration of metaphase in *rts1-AID* cells was somewhat shorter in rich carbon compared to poor carbon, the difference was barely significant (p-value = 0.025). In contrast, the difference in metaphase duration between rich and poor carbon in wild type cells was highly significant (p-value = 0.000002) (**Figure S2B**). Together, these observations suggest that *rts1-AID* caused defects in nutrient modulation of metaphase duration, despite the fact that *rts1-AID* caused only a partial loss of function. There was a statistically significant decrease in the duration of anaphase in rich carbon in *rts1-AID* cells, which could again be due to partial function of *rts1-AID* (**Figure 7A,B**)

rts1-AID caused a large increase in daughter bud size at all stages of mitosis in both rich and poor carbon (**Figures 7C,D**; see **Figures S4C,D** for dot plots and p-values). The variance in size at the end of metaphase was much larger in *rts1-AID* cells compared to wild type cells. In addition, there was not a statistically significant difference in the size of *rts1-AID* cells in rich or poor carbon at the end of metaphase. By the end of anaphase, *rts1-AID* cells in rich carbon were slightly larger than their counterparts in poor carbon.

Inactivation of PP2A^{Rts1} disrupts the normal relationship between growth rate and size

Destruction of rts1-AID reduced the growth rate by approximately 30% in both rich and poor carbon (**Figure 7E;** see **Figure S4E** for dot plots and p-values). Under normal circumstances, a reduced growth rate causes a reduced cell size, whereas destruction of rts1-AID causes a reduced growth rate, but an increase in size. More importantly, the correlation between growth rate and daughter cell size was largely lost in *rts1-AID* cells (**Figure 7F**). Thus, buds with nearly identical growth rates completed mitosis at very different sizes. Together, these observations demonstrate that inactivation of PP2A^{Rts1} disrupts the normal relationship between growth rate and size.

The increased duration of mitosis in poor carbon is partially due to Cdk1 inhibitory phosphorylation

We next searched for targets of PP2A^{Rts1} that control mitotic duration and daughter cell size. In a previous study we identified candidate targets of PP2A^{Rts1} by using proteome-wide mass spectrometry to search for proteins that are hyperphosphorylated in *rts1*Δ cells (Zapata et al., 2014). The analysis identified multiple proteins in a pathway that delays mitosis via inhibitory phosphorylation of Cdk1. In this pathway, Swe1, the budding yeast homolog of Wee1, phosphorylates and inhibits Cdk1 (Gould and Nurse, 1989; Booher et al., 1993). The most strongly hyperphosphorylated site identified in *rts1*Δ cells was the inhibitory site on Cdk1 targeted by Swe1. The analysis also showed that multiple sites on Swe1 that play a role in its activation are hyperphosphorylated in *rts1*Δ cells, which suggests that Swe1 is hyperactive (Harvey et al., 2005; 2011). Finally, the analysis identified two related kinases, Gin4 and Hsl1, that inhibit Swe1 via poorly understood mechanisms (Ma et al., 1996; Barral et al., 1999; McMillan et al., 1999; Longtine et al., 2000). Thus, the mass spectrometry data established that PP2A^{Rts1} works in a pathway that controls mitotic Cdk1 inhibitory phosphorylation.

Although inhibitory phosphorylation of Cdk1 was originally thought to control entry into mitosis, more recent work found that metaphase is shortened in *swe1*Δ cells (Lianga et al., 2013; Raspelli et al., 2014). Moreover, overexpression of Swe1, or inactivation of Gin4, causes cells to undergo prolonged delays in metaphase (Raspelli et al., 2014; Altman and Kellogg, 1997; Booher et al., 1993). Together, these observations suggest that inhibitory phosphorylation of Cdk1 influences the duration of mitotic events after entry into mitosis, which led us to hypothesize that lengthening of mitosis in poor carbon is due, at least in part, to inhibitory phosphorylation of Cdk1 by Swe1. To test this, we first used a phospho-specific antibody to determine whether Cdk1 inhibitory phosphorylation is prolonged in poor carbon.

Cells growing in either rich or poor carbon were released from a G1 arrest and samples were taken at 15 minute intervals for western blot analysis with antibodies that detect Clb2 and Cdk1 inhibitory phosphorylation. Cdk1 inhibitory phosphorylation was prolonged in poor carbon and closely paralleled Clb2 levels throughout most of mitosis (**Figures 1A** and **8A;** western blots in both figures are from the same samples). These observations suggest that Cdk1 inhibitory phosphorylation can persist well beyond entry into mitosis, and that it could play a role in the lengthening of mitosis in poor nutrients.

We also analyzed the behavior of Swe1 during the cell cycle in rich and poor carbon. Swe1 passes through multiple phosphorylation states during mitosis that can be detected via electrophoretic mobility shifts; attainment of a fully hyperphosphorylated state is correlated with inactivation of Swe1 (Sreenivasan and Kellogg, 1999; McMillan et al., 2002; Raspelli et al., 2011; Harvey et al., 2011). In rich media, Swe1 reached full hyperphosphorylation and was degraded shortly thereafter (**Figure 8B**). In poor media, Swe1 was present throughout most of the prolonged mitosis. Moreover, Swe1 took longer to reach the fully hyperphosphorylated state, and it persisted in the partially hyperphosphorylated state that is thought to represent the active form of Swe1. These observations suggest that signals that control Swe1 could play a role in prolonging Cdk1 inhibitory phosphorylation in poor nutrients.

The role of Swe1 was further characterized by analyzing daughter cell growth and mitotic events in single cells. In rich carbon, *swe1*Δ caused a slight reduction in the average duration of metaphase, as previously described (**Figure 9A;** see **Figure S5A** for dot plots and p-values). In poor carbon, *swe1*Δ caused a greater reduction in metaphase duration, from 34 minutes to 29 minutes (**Figure 9B)**. Although *swe1*Δ reduced the duration of metaphase in poor carbon, it did not reduce it to the duration observed for wild type cells in rich carbon, which indicates that the mitotic delay in poor carbon is not due solely to inhibitory phosphorylation of Cdk1.

In both rich and poor carbon, *swe1*Δ caused a reduction in growth rate (**Figure 9C**). This, combined with the reduced duration of metaphase, caused *swe1*Δ daughter buds to undergo each of the mitotic transitions at a significantly reduced size in both rich and poor carbon (**Figures 9D,E;** see **Figures S5C,D** for dot plots and p-values). Together, the data demonstrate that Swe1 plays a role in the increased duration of mitosis in poor carbon and is required for normal control of daughter cell size at cytokinesis.

PP2A^{Rts1} controls the duration of mitosis by Swe1-dependent and Swe1-independent mechanisms

We next tested whether PP2A^{Rts1} controls mitotic duration and daughter cell size via Swe1. Western blot assays confirmed that destruction of rts1-AID in synchronized cells caused a prolonged mitotic delay in both rich and poor carbon (**Figure 10A**). The delay was reduced, but not eliminated, by *swe1*Δ. We also found that *rts1*Δ caused a mitotic delay after release from a metaphase arrest that was largely reduced by *swe1*Δ, but not fully eliminated (**Figure 10B**).

In single cell assays, the delays in metaphase caused by *rts1-AID* in rich and poor carbon were largely reduced by *swe1*Δ, but not fully eliminated (**Figures 11A,B;** see **Figures S5E,F** for dot plots and p-values). The increased duration of anaphase caused by *rts1-AID* in rich and poor carbon was largely unaffected by *swe1*Δ. Although *swe1*Δ did not fully rescue the mitotic delay caused by *rts1-AID*, it caused *rts1-AID* cells to exit mitosis at a size similar to that of *swe1*Δ cells (**Figures 11C,D;** see **Figures S5G,H** for dot plots and p-values). This was a combined result of the reduction in mitotic duration and a decrease in growth rate in *rts1-AID swe1*Δ cells relative to *rts1-AID* or *swe1*Δ cells (**Figures 7C, 9C** and **11E**). Together, these observations demonstrate that PP2A^{Rts1} controls mitotic duration and daughter cell size via a Swe1-dependent pathway, as well as a Swe1-independent pathway.

Discussion

Daughter cell size and the duration of mitosis are modulated by nutrients

Daughter cells are born at a significantly smaller size in poor nutrients (Johnston et al., 1977). To explain this observation, it has been suggested that the average duration of bud growth is invariant, even when growth rate is reduced by poor nutrients (Johnston et al., 1977). This would suggest that the reduced size of daughter cells in poor nutrients is a simple consequence of reduced growth rate. We tested this model by simultaneously monitoring bud growth and cell cycle events, which revealed that the duration of daughter bud growth is not invariant. Rather, poor carbon causes a significant increase in the duration of daughter bud growth during mitosis. Despite the increased duration of mitosis, daughter cells growing in poor carbon are born at almost half the size of cells in rich carbon. Together, these observations suggest that cell size checkpoint mechanisms control the extent of growth during mitosis, and that the amount of growth required to pass the checkpoints is reduced in poor carbon, resulting in production of small daughter cells.

The fact that most cell growth occurs during a rapid growth phase in mitosis suggests that maintenance of a specific cell size requires tight control over the interval of mitotic growth. For example, a 20% change in the duration of growth in mitosis would have a large effect on cell size, whereas a 20% change in the duration of growth in G1 phase would have little effect. Similarly, modulation of the duration of G1 phase seems unlikely to play a dominant role in control of cell size because so little growth occurs during G1 phase, and the rate of growth is significantly slower. Rather, since most growth in volume occurs in mitosis, it would make sense that cells control their size primarily by controlling the extent of growth during mitosis. The existence of major cell size control mechanisms in mitosis would explain why cells lacking Whi5, as well as other critical regulators of the G1 size checkpoint, still show robust nutrient modulation of cell size (Jorgensen et al., 2004).

A number of observations suggest that the increased duration of mitosis in poor carbon is a response to reduced growth rate. Cells shifted from rich to poor carbon during metaphase undergo a prolonged mitotic delay, whereas cells shifted during anaphase do not. If the delay were a consequence of a reduction in ATP or other metabolites needed for mitotic spindle events, one would expect to see delays in both metaphase and anaphase. Rather, we hypothesize that a shift to poor carbon during metaphase causes a delay because the daughter bud has not yet undergone sufficient growth, whereas a shift in anaphase does not cause a delay because buds have already undergone extensive growth and have reached the threshold amount of growth needed to complete mitosis in poor carbon.

More evidence for mitotic cell size control comes from the discovery that Swe1 and $PP2A^{Rts1}$ control mitotic duration and cell size at completion of mitosis. $PP2A^{Rts1}$ was previously implicated in cell size control and is required for nutrient modulation of cell size (Artiles et al., 2009; Zapata et al., 2014). Similarly, inhibitory phosphorylation of Cdk1 by Wee1-family members has been implicated in cell size control for over three decades (Nurse, 1975; Harvey and Kellogg, 2003; Jorgensen et al., 2002). The involvement of Cdk1 inhibitory phosphorylation and $PP2A^{Rts1}$ is therefore consistent with a model in which increased duration of mitosis in poor carbon is a regulated event, rather than a non-specific consequence of metabolic changes caused by poor carbon.

An alternative model could be that the duration of mitosis is controlled by a nutrient modulated timer. In rich media, the timer would be set for a short duration of growth, while in poor media it would be set for a longer interval. Because metaphase cells shifted from rich to poor carbon undergo a delay, but anaphase cells do not, the timer would have to be metaphase specific and could not account for the delay in anaphase caused by poor nutrients. A timer model could explain the correlation between growth rate and cell size, since cells with a higher growth rate should complete a growth interval at a larger size. However, the timer model does

not seem consistent with the large variance in mitotic duration between individual cells growing under identical conditions.

The rate of growth is modulated during the cell cycle

Building on previous studies, we observed dramatic changes in the rate of growth during the cell cycle. Bud growth prior to mitosis occurs at a slow rate, but once cells enter mitosis the rate of growth increases approximately 4-fold in rich carbon and 2-fold in poor carbon. As cells exit mitosis and enter G1 phase, growth slows and remains slow through G1 phase. Thus, growth cannot be considered a simple monotonic function that is independent of the cell cycle. Rather, the rate, duration, extent, and location of cell growth are all regulated during the cell cycle. Previous studies have shown that polar bud growth is dependent upon Cdk1 activity, but the signals that control bud growth at other stages of the cell cycle are unknown (McCusker et al., 2007). Moreover, the mechanisms and function of growth rate modulation during the cell cycle are unknown.

Control of mitotic duration and cell size at completion of mitosis

In previous studies, we found that $PP2A^{Rts1}$ is required for nutrient modulation of cell size (Artiles et al., 2009). A proteome-wide search for targets of $PP2A^{Rts1}$-dependent regulation identified multiple potential effectors of cell size checkpoints, including proteins that control mitotic events (Zapata et al., 2014). Since known effectors of G1 cell size checkpoints are not required for nutrient modulation of cell size (Jorgensen et al., 2004), these observations led us to hypothesize that nutrient modulation of cell size occurs primarily in mitosis, and that $PP2A^{Rts1}$ plays an important role. Here, we tested this hypothesis by analyzing how loss of $PP2A^{Rts1}$ affects cell growth and size throughout mitosis. This revealed that a partial loss of function of $PP2A^{Rts1}$ causes severe defects in mitotic duration and cell size at completion of mitosis. We further established that $PP2A^{Rts1}$ influences mitotic duration, in part, by controlling Cdk1 inhibitory phosphorylation. Previous work in budding yeast, Drosophila and human cells also reached the conclusion that Cdk1 inhibitory phosphorylation controls the duration of mitotic events after mitotic entry (Jin et al., 2008; Lianga et al., 2013; Raspelli et al., 2014; Toledo et al., 2015).

Although *swe1*Δ significantly reduced the metaphase delays caused by partial inactivation of $PP2A^{Rts1}$ or poor nutrients, it had little effect on anaphase delays. In addition, *swe1*Δ did not reduce metaphase duration in cells growing in poor nutrients or *rts1-AID* cells to match metaphase duration of wild type cells in rich nutrients. Together, these observations indicate that mitotic delays caused by poor nutrients or inactivation of $PP2A^{Rts1}$ are not due solely to Cdk1 inhibitory phosphorylation. A recent study in fission yeast also reached the conclusion that there are major Wee1-independent mechanisms for controlling cell size in mitosis (Wood and Nurse, 2013).

Our mass spectrometry analysis of *rts1*Δ cells identified a number of additional targets of $PP2A^{Rts1}$ that could control mitotic duration (Zapata et al., 2014). A particularly interesting candidate is Pds1, also referred to as securin. Pds1 binds and inhibits separase, the protease that initiates chromosome segregation via proteolytic cleavage of cohesins. Previous studies have shown that Pds1 is regulated, and that it controls progression through both metaphase and anaphase (Wang et al., 2001; Tinker-Kulberg and Morgan, 1999; Holt et al., 2008). Thus, $PP2A^{Rts1}$-dependent control of Pds1 could play a role in controlling the duration of mitosis. Pds1 plays both positive and negative roles in controlling separase, so *pds1*Δ causes a complex phenotype (Yamamoto et al., 1996; Ciosk et al., 1998; Jensen et al., 2001). Thus, we were not able to test whether *pds1*Δ reduces delays caused by poor nutrients or *rts1-AID*. The mass spectrometry analysis of *rts1*Δ also identified numerous components of the mitotic exit network, which suggests another mechanism by which $PP2A^{Rts1}$ could control mitotic duration. $PP2A^{Rts1}$

is localized to kinetochores, so it is well-positioned to control the rate of mitotic spindle events (Dobbelaere et al., 2003).

Cell size is proportional to growth rate

Previous studies found that cell size at the end of G1 phase is proportional to growth rate during G1 phase: rapidly growing cells complete G1 phase at a larger size than slow growing cells (Ferrezuelo et al., 2012; Johnston et al., 1979). Similarly, we found that cell size at the end of mitosis is proportional to growth rate during mitosis. Thus, cell size at all key cell cycle transitions is correlated with growth rate. The correlation holds when comparing different cells growing under the same conditions, and when comparing different populations of cells growing under different nutrient conditions.

If cell size is proportional to growth rate, faster growing cells should always give rise to larger daughter cells. And since growth rate is proportional to size, larger daughter cells should have a higher growth rate, leading to ever larger daughter cells. In this case, what limits cell size? A plot of daughter cell size at cytokinesis as a function of mother cell size revealed that daughter cell size indeed increases with mother cell size, but the ratio of mother size to daughter size is not constant across the range of mother cell sizes (**Figure 5B**). In other words, very large mothers produce daughters that are nearly half the size of the mother, while small mothers produce daughters of nearly equal size (Johnston et al., 1977). This relationship would correct large variations in mother cell size, which could be the result of growth during cell cycle delays induced by other checkpoints, such as the spindle checkpoint or DNA damage checkpoints. Variation in mother cell size could also be the product of noisy cell size checkpoint mechanisms.

The strong correlation between growth rate and cell size is difficult to reconcile with a simple cell size checkpoint model in which a threshold volume must be reached to pass the checkpoint. If a specific volume must be reached to pass a checkpoint, the rate at which the cell reaches that volume should not influence the final volume at which the cell passes the checkpoint. One way to reconcile the idea of a set threshold volume with growth rate dependence would be to imagine that cell size checkpoint thresholds are noisy and imperfect. In this view, faster growing cells will overshoot the threshold size more than slow growing cells, leading to increased size. This model would not explain nutrient modulation of cell size.

Another explanation for the relationship between cell size and growth rate could be that cells measure their growth rate and set cell size checkpoint thresholds to match the current growth rate. Alternatively, the same signals that set the growth rate could also set the cell size threshold. Both models would explain nutrient modulation of cell size, since nutrients modulate growth rate. Several observations are consistent with a close functional relationship between growth rate and cell size. Inactivation of $PP2A^{Rts1}$ caused a reduced growth rate, which suggests that it operates in signaling pathways that control growth rate. The defects in the growth rate of the bud in *rts1-AID* cells cannot be secondary consequence of defects in mother cell size, since we observed the immediate effects of loss of $PP2A^{Rts1}$ in cells with normal mother cell size. In addition, *rts1-AID* cells showed a reduced growth rate, but completed mitosis at a much larger daughter cell size. This demonstrates that the effects of *rts1-AID* are not a secondary consequence of reduced growth rate, since one would expect this to cause a reduced cell size. Most importantly, *rts1-AID* almost completely abolished the normal linear relationship between growth rate and cell size, and caused *rts1-AID* cells to complete mitosis at an abnormally wide range of bud sizes. The fact that *rts1-AID* simultaneously causes defects in growth rate, coordination of cell size with growth rate, and cell size at completion of mitosis, provides strong support for a model in which common signals coordinately set growth rate and cell size, and suggest that $PP2A^{Rts1}$ plays a central role in these signals. Further investigation of the signals that act upstream and downstream of $PP2A^{Rts1}$ should provide important clues to how cell size is controlled.

Materials and Methods

Yeast strains and media

The genotypes of the strains used in this study are listed in Table 1. All strains are in the W303 background (*leu2-3,112 ura3-1 can1-100 ade2-1 his3-11,15 trp1-1 GAL+, ssd1-d2*). Genetic alterations were carried out using one-step PCR-based integration at the endogenous locus (Longtine et al., 1998; Janke et al., 2004).

For cell cycle time courses and analysis of cell size by Coulter counter, cells were grown in YP media (1% yeast extract, 2% peptone, 8ml/L adenine) supplemented with 2% dextrose (YPD), or with 2% glycerol and 2% ethanol (YPGE). For microscopy, cells were grown in complete synthetic media (CSM) with 2% dextrose (CSM-Dex) or 2% glycerol and 2% ethanol (CSM-G/E).

Table 1

Strain	MAT	Genotype*
DK186	a	*bar1*
DK2423	a	*bar1, TIR1::LEU2, TIR1::HIS3, rts1-AID::KanMX6*
DK2523	a	*bar1, SPC42-GFP::HIS3, MYO1-GFP::TRP*
DK2879	a	*bar1, TIR1::LEU2, TIR1::HIS3, SPC42-GFP::hphNT1, MYO1-GFP:KITRP, rts1-AID::KanMX6*
DK2930	a	*bar1, SPC42-GFP::HIS3, MYO1-GFP::TRP, swe1Δ::URA3*
DK3072	a	*bar1, TIR1::LEU2, TIR1::HIS3, SPC42-GFP::hphNT1, MYO1-GFP::KITRP, rts1-AID::KanMX6, swe1Δ::URA3*
DK1993	a	*bar1, GAL1-CDC20::NatNT2*
DK2176	a	*bar1, GAL1-CDC20::NatNT2, rts1::KanMX4*
DK2243	a	*bar1, GAL1-CDC20::NatNT2, rts1::KanMX4, swe1::URA3*

***** All strains are in the W303 background (*leu2-3,112 ura3-1 can1-100 ade2-1 his3-11,15 trp1-1 GAL+ ssd1-d2*)

Microscopy

Cells were grown overnight in CSM-Dex or CSM-G/E at room temperature with constant rotation to an optical density near 0.1 at λ600. 5 ml of culture were arrested with α factor at 0.5 µg/ml for 3-4 hours. Cells were released from the arrest by 3 consecutive washes with the same media and re-suspended in 500 µl of media. Approximately 200 µl of cell suspension were spotted on a concanavalin A-treated glass bottom dish with a 10 mm micro-well #1.5 cover glass. Cells were adhered for 5 min and unbound cells were washed away by repeated washing with 1 ml pre-warmed media. The dish was then flooded with 3 ml of media and placed on a temperature controlled microscope stage set to 27°C (Pecon Tempcontrol 37-2 digital). The temperature of the media was monitored throughout the experiment using a MicroTemp TQ1 reader coupled to a Teflon insulated K-type thermocouple (Omega). The probe was placed in contact with the glass bottom near the contact area between the objective and the dish. Temperature was maintained at 27 $^{+}/_{-}$ 1°C; imaging sessions where the temperature varied beyond this limit were rejected from final analysis. Brightfield and fluorescent images were acquired simultaneously using a Zeiss LSM 5 Pascal microscope and a Plan-Apochromat 63x/1.4 oil objective. 488nm light was obtained from an argon laser light source using a (488/543/633) primary dichroic beam splitter (HFT). The laser was set to 0.7% intensity. For green fluorescence images, light was collected through a long pass 505 emission filter using a 1 AU size pinhole. Brightfield images were collected using the transmitted light detector. Optical sections were taken for a total of 11 z-planes every 0.5 µm with frame averaging set to 2, to

reduce noise. The total exposure was kept as low as possible to reduce photo-damage (1.60 µs dwell time per pixel, image dimension set to 512 x 512 px, and pixel size set to 0.14 x 0.14 µm). Images were acquired at 3 min intervals for rich carbon and 4 min intervals for poor carbon, with the exception of *rts1-AID* mutants in poor carbon, which were imaged every 6 min to compensate for the greatly increased cell cycle duration. Conditional degradation of rts1Δ-AID was achieved by addition of auxin to 1 mM from a 50 mM stock. Auxin was added 20 min after release from G1 arrest for rich carbon and 60 min after release for poor carbon.

Image analysis

Image analysis was performed using ImageJ (Schneider et al., 2012; Linkert et al., 2010). The ImageJ plug-ins StackReg and MultiStackReg were used for post-acquisition image-stabilization (Thevenaz et al., 1998; Busse). Stabilized bright-field images were processed using the imageJ plug-in FindFocusedSlices and the volume of growing buds was determined using BudJ, a plugin for ImageJ (Tseng; Ferrezuelo et al., 2012). Bud volumes were measured for buds whose focal plane was no more than 1.5 µm away (3 z-steps) from their mother's focal plane. Sum projections of z-stacks were treated using a 2 px mean filter, and brightness/contrast levels were adjusted to reduce background noise. The treated pseudo-colored green fluorescent images were overlapped with the outlines of the imaged cells for reference (outlines were generated using the "find edges" command over a sum projection of all z-stacks of bright field images). Positions of spindle poles (SPBs) were determined using the crosshair tool (set to auto-measure and auto-next) and distance between the 2 SPBs was determined using the mathematical formula for the distance between 2 points. Disappearance of the Myo1 ring was determined empirically by observation of GFP signal at the bud neck.

Statistical analysis

Data acquired from ImageJ was analyzed using Apple Numbers, R (The R Core Team, 2016), RStudio (RStudio Team, 2015), and the R package ggplot2 (Wickham, 2009). p-values were calculated using a Welch Two Sample t-test and a 95% confidence interval.

Cell cycle time courses

For western blot time courses, cells were grown overnight at room temperature in liquid YPD or YPGE to an optical density of 0.5 at λ600. Because optical density is affected by cell size, we normalized cell numbers by counting cells with a Coulter counter (Beckman Coulter) when comparing cells grown in rich or poor carbon.

G1 synchronization was achieved by arresting cells with α factor at a concentration of 0.5 µg/ml until at least 90% of cells were unbudded. Cells were released from the arrest by washing 3× with fresh media. Time courses were performed at 25ºC with constant agitation. To prevent cells from re-entering the following cell cycle α factor was added back after most cells had budded. For nutrient shift time courses a single culture was arrested and split at the moment of release from the G1 arrest. At the time of the shift both cultures were washed 3× by centrifugation with room temperature YPD (control) or YPGE (shifted cells). The volume of the culture was restored to its original volume prior to the washes and cultures were placed back at 25ºC.

To arrest cells in mitosis, *GAL1-CDC20* cells were grown overnight in YP media containing 2% raffinose and 2% galactose and arrested by washing into YP containing 2% raffinose. Cells were monitored until all cells had large buds. Cells were released from metaphase by re-addition of 2% galactose.

For western blots 1.6 ml samples were collected at regular intervals, pelleted and flash frozen in presence of 200 µl of glass beads. For immunofluorescence analysis of mitotic spindles, 800 µl of culture were collected alongside western blot samples into tubes containing 88 µl of paraformaldehyde. After fixation for 1-2 hours, cells were pelleted and washed 3× with

PBS that contains 0.05%Tween-20 and 0.02% sodium azide (PBST) and stored at 4°C for up to 2 days before analysis. Mitotic spindles were labelled by immunofluorescence as previously described (Pringle et al., 1991).

Western blotting

Cell lysis and western blotting were carried out as previously described (Harvey et al., 2005). Briefly, cells were lysed in a Multibeater-16 (BioSpec Products, Inc.) at top speed for 2 min in the presence of 165 µl of sample buffer (65 mM Tris-HCl, pH 6.8, 3% SDS, 10% glycerol, 50 mM NaF, 100 mM glycerolphosphate, 5% 2-mercaptoethanol, and bromophenol blue). PMSF was added to the sample buffer to a final concentration of 2 mM immediately before cell lysis. After lysis, samples were centrifuged for 2 min at 13,000 rpm and placed in a boiling water bath for 7 min. After boiling, the samples were centrifuged for 2 min at 13,000 rpm and loaded on an SDS polyacrylamide gel.

SDS-PAGE was performed at a constant current of 20 mA. For Clb2, Swe1 and Rts1 blots, electrophoresis was performed on 10% polyacrylamide gels until a 43-kD pre-stained marker ran to the bottom of the gel. For Cdk1-Y19 blots 12.5% gels were used and gels were run until a 14.4-kD marker was at the bottom of the gel. Proteins were transferred onto nitrocellulose membranes for either 75 min at 800 mA at 4°C in a TE22 transfer tank (Hoeffer) in buffer containing 20 mM Tris base, 150 mM glycine, and 20% methanol, or for 7 min using Trans-Blot® Turbo™ Transfer System (Bio-Rad) using proprietary transfer buffer.

Blots were probed overnight at 4°C with affinity-purified rabbit polyclonal antibodies raised against Clb2, Swe1 and Rts1. Cdk1 phosphorylated at tyrosine 19 was detected using a phospho-specific antibody (Cell Signaling Technology, cat# 10A11). All blots were probed with HRP-conjugated donkey anti-rabbit secondary antibody (GE Healthcare, cat# NA934) for 75 min at room temperature. Secondary antibodies were detected via chemiluminescence using WesternBright ECL or Quantum substrate (Advansta). Blots were exposed to film or imaged using a ChemiDoc™ MP System (Bio-Rad). For quantification of rts1-AID degradation, band intensity was quantified using ImageLab™.

Spindle staining and counting

Fixed cells were treated for immunofluorescence as previously described using rat anti-tubulin primary antibody followed by goat anti-rat FITC-conjugated antibody (Sigma-Aldrich, Cat# F1763) (Pringle et al., 1991). Multi-plane imaging of slides was performed using a Leica DM5500 B Widefield Microscope and a 63x/ 0.6-1.4 oil objective. Spindles were counted in ImageJ. Data was processed and plotted using Apple Numbers.

Supplemental Material

Figure S1. Growth curve data for cells growing in rich or poor carbon. Blue highlighting represents metaphase, pink represents anaphase, and yellow represents G1 phase. Curves where yellow is absent are from cells that could not be followed through a complete G1 phase or where the timing of the appearance of the daughter bud could not be determined with confidence. **(A)** Growth curves for cells growing in rich carbon. Curves for all 32 measured cells are shown. (**B**) Growth curves for cells growing in poor carbon. Several curves were omitted because they yielded clear data for one stage of mitosis, but not for others, due to imaging limitations. Data from these curves were used if they yielded high confidence data for one of the mitotic stages.

Figure S2. Dot plot versions of the data used to generate Figure 3. Black horizontal lines and adjacent numbers represent the average value for the data in each dot plot. The significance of the difference between two conditions is given as p-values above each plot. **(A)** Dot plot version of the data used to generate Figures 3A and 3B. (**B)** Dot plot versions of the data used to generate Figure 3C.

Figure S3. Characterization of *rts1-AID* cells. (**A**) The size of wild type and *rts1-AID* cells grown to log phase in liquid YPD cultures was measured with a Coulter counter. (**B**) Wild type and *rts1-AID* cells were released from a G1 arrest in YPGE and the timing of entry into mitosis and the duration of mitosis were determined by assaying levels of the mitotic cyclin Clb2 by western blot. (**C**) *rts1-AID* cells were released from a G1 arrest in YPD and auxin was added at 60 minutes. Destruction of rts1-AID was assayed by western blot. The average rts1-AID signal was measured using BioRad Imagelab™ for 3 biological replicates and the mean percent of rts1-AID protein remaining at each time point is listed below each lane. (**D**) The rate of proliferation of *rts1Δ* and *rts1-AID* cells was tested by spotting a series of 10-fold dilutions of each strain on YPD+auxin at 34ºC.

Figure S4. Dot plot versions of the data used to generate Figure 7. Black horizontal lines and adjacent numbers represent the average value for the data in each dot plot. The significance of the difference between two conditions or genotypes is given as p-values below each bracket. **(A)** Dot plot versions of the data used to generate Figures 7A. **(B)** Dot plot versions of the data used to generate Figure 7B. **(C)** Dot plot versions of the data used to generate Figure 7C. **(D)** Dot plot versions of the data used to generate Figure 7D. **(E)** Dot plot versions of the data used to generate Figure 7E.

Figure S5. Dot plot versions of the data used to generate Figures 9 and 11. Black horizontal lines and adjacent numbers represent the average value for the data in each dot plot. The significance of the difference between two conditions or genotypes is given as p-values below each bracket. **(A,B)** Dot plot versions of the data used to generate Figures 9A and 9B. **(C,D)** Dot plot versions of the data used to generate Figure 9D and 9E. **(E,F)** Dot plot versions of the data used to generate Figures 11A and 11B. **(G,H)** Dot plot versions of the data used to generate Figures 11C and 11D.

Acknowledgments

We thank Ben Abrams, Facilities Manager for the UCSC Life Sciences Microscopy Center for support and mentoring with all microscopy related techniques, and the Aldea lab for sharing BudJ: an ImageJ plugin to analyze images of budding yeast cells (http://www.ibmb.csic.es/home/maldea). R.L. was supported by a fellowship from the "Fundação para a Ciência e a Tecnologia" (FCT), with funds from "Programa Operacional Potencial Humano/ Fundo Social Europeu" (POPH/FSE), under the fellowship SFRH/BD/75004/2010. This work was supported by National Institutes of Health Grant R01-GM053959.

References

Altman, R., and D.R. Kellogg. 1997. Control of Mitotic Events by Nap1 and the Gin4 Kinase. *J. Cell Biol.* 138:119–130. doi:10.1083/jcb.138.1.119.

Artiles, K., S.D. Anastasia, D. McCusker, and D.R. Kellogg. 2009. The Rts1 Regulatory Subunit of Protein Phosphatase 2A Is Required for Control of G1 Cyclin Transcription and Nutrient Modulation of Cell Size. *PLoS Genet*. 5:e1000727 EP –. doi:10.1371/journal.pgen.1000727.

Barral, Y., M. Parra, S. Bidlingmaier, and M. Snyder. 1999. Nim1-related kinases coordinate cell cycle progression with the organization of the peripheral cytoskeleton in yeast. *Genes & Development*. 13:176–187.

Barral, Y., S. Jentsch, and C. Mann. 1995. G1 cyclin turnover and nutrient uptake are controlled by a common pathway in yeast. *Genes & Development*. 9:399–409. doi:10.1101/gad.9.4.399.

Booher, R.N., R.J. Deshaies, and M.W. Kirschner. 1993. Properties of Saccharomyces cerevisiae wee1 and its differential regulation of p34CDC28 in response to G1 and G2 cyclins. *EMBO J.* 12:3417–3426.

Busse, B. MultiStackReg V1.45. http://bradbusse.net/downloads.html.

Ciosk, R., W. Zachariae, C. Michaelis, A. Shevchenko, M. Mann, and K. Nasmyth. 1998. An ESP1/PDS1 Complex Regulates Loss of Sister Chromatid Cohesion at the Metaphase to Anaphase Transition in Yeast. *Cell*. 93:1067–1076. doi:10.1016/S0092-8674(00)81211-8.

Costello, G., L. Rodgers, and D. Beach. 1986. Fission yeast enters the stationary phase G0 state from either mitotic G1 or G2. *Curr Genet*. 11:119–125. doi:10.1007/BF00378203.

Cross, F.R. 1988. DAF1, a mutant gene affecting size control, pheromone arrest, and cell cycle kinetics of Saccharomyces cerevisiae. *Mol. Cell. Biol.* 8:4675–4684. doi:10.1128/MCB.8.11.4675.

Cross, F.R. 1990. Cell cycle arrest caused by CLN gene deficiency in Saccharomyces cerevisiae resembles START-I arrest and is independent of the mating-pheromone signalling pathway. *Mol. Cell. Biol.* 10:6482–6490. doi:10.1128/MCB.10.12.6482.

Dobbelaere, J., M.S. Gentry, R.L. Hallberg, and Y. Barral. 2003. Phosphorylation-dependent regulation of septin dynamics during the cell cycle. *Developmental Cell*. 4:345–357. doi:10.1016/S1534-5807(03)00061-3.

Fantes, P., and P. Nurse. 1977. Control of cell size at division in fission yeast by a growth-modulated size control over nuclear division. *Exp. Cell Res.* 107:377–386.

Farkaš, V., J. Kovařík, A. Košinová, and Š. Bauer. 1974. Autoradiographic study of mannan incorporation into the growing cell walls of Saccharomyces cerevisiae. *J. Bacteriol.* 117:265–269.

Ferrezuelo, F., N. Colomina, A. Palmisano, E. Garí, C. Gallego, A. Csikász-Nagy, and M. Aldea. 2012. The critical size is set at a single-cell level by growth rate to attain homeostasis and

adaptation. *Nat Commun*. 3:1012–11. doi:10.1038/ncomms2015.

Goranov, A.I., M. Cook, M. Ricicova, G. Ben-Ari, C. Gonzalez, C. Hansen, M. Tyers, and A. Amon. 2009. The rate of cell growth is governed by cell cycle stage. *Genes & Development*. 23:1408–1422. doi:10.1101/gad.1777309.

Gould, K.L., and P. Nurse. 1989. Tyrosine phosphorylation of the fission yeast cdc2+ protein kinase regulates entry into mitosis. *Nature*. 342:39–45. doi:10.1038/342039a0.

Hartwell, L.H., and M.W. Unger. 1977. Unequal division in Saccharomyces cerevisiae and its implications for the control of cell division. *The Journal of Cell Biology*. 75:422–435. doi:10.1083/jcb.75.2.422.

Harvey, S.L., A. Charlet, W. Haas, S.P. Gygi, and D.R. Kellogg. 2005. Cdk1-Dependent Regulation of the Mitotic Inhibitor Wee1. *Cell*. 122:407–420. doi:10.1016/j.cell.2005.05.029.

Harvey, S.L., and D.R. Kellogg. 2003. Conservation of Mechanisms Controlling Entry into Mitosis: Budding Yeast Wee1 Delays Entry into Mitosis and Is Required for Cell Size Control. *Current Biology*. 13:264–275. doi:10.1016/S0960-9822(03)00049-6.

Harvey, S.L., G. Enciso, N.E. Dephoure, S.P. Gygi, J. Gunawardena, and D.R. Kellogg. 2011. A phosphatase threshold sets the level of Cdk1 activity in early mitosis in budding yeast. *Molecular Biology of the Cell*. 22:3595–3608. doi:10.1091/mbc.E11-04-0340.

Holt, L.J., A.N. Krutchinsky, and D.O. Morgan. 2008. Positive feedback sharpens the anaphase switch. *Nature*. 454:353–357. doi:10.1038/nature07050.

Janke, C., M.M. Magiera, N. Rathfelder, C. Taxis, S. Reber, H. Maekawa, A. Moreno-Borchart, G. Doenges, E. Schwob, E. Schiebel, and M. Knop. 2004. A versatile toolbox for PCR-based tagging of yeast genes: new fluorescent proteins, more markers and promoter substitution cassettes. *Yeast*. 21:947–962. doi:10.1002/yea.1142.

Jensen, S., M. Segal, D.J. Clarke, and S.I. Reed. 2001. A Novel Role of the Budding Yeast Separin Esp1 in Anaphase Spindle Elongation: Evidence That Proper Spindle Association of Esp1 Is Regulated by Pds1. *The Journal of Cell Biology*. 152:27–40. doi:10.1083/jcb.152.1.27.

Jin, Z., E. Homola, S. Tiong, and S.D. Campbell. 2008. Drosophila myt1 is the major cdk1 inhibitory kinase for wing imaginal disc development. *Genetics*. 180:2123–2133. doi:10.1534/genetics.108.093195.

Johnston, G.C., C.W. Ehrhardt, A. Lorincz, and B.L.A. Carter. 1979. Regulation of cell size in the yeast Saccharomyces cerevisiae. *J. Bacteriol.* 137:1–5.

Johnston, G.C., J.R. Pringle, and L.H. Hartwell. 1977. Coordination of growth with cell division in the yeast Saccharomyces cerevisiae. *Exp. Cell Res.* 105:79–98. doi:doi: 10.1016/0014-4827(77)90154-9.

Jorgensen, P., and M. Tyers. 2004. How Cells Coordinate Growth and Division. *Current Biology*. 14:R1014–R1027. doi:10.1016/j.cub.2004.11.027.

Jorgensen, P., I. Rupes, J.R. Sharom, L. Schneper, J.R. Broach, and M. Tyers. 2004. A dynamic transcriptional network communicates growth potential to ribosome synthesis and critical cell size. *Genes & Development*. 18:2491–2505. doi:10.1101/gad.1228804.

Jorgensen, P., J.L. Nishikawa, B.-J. Breitkreutz, and M. Tyers. 2002. Systematic Identification of Pathways That Couple Cell Growth and Division in Yeast. *Science*. 297:395–400. doi:10.1126/science.1070850.

Kimball, R.F., and L. Vogt-Köhne. 1961. Quantitative cytochemical studies on Paramecium aurelia. *Exp. Cell Res.* 23:479–487. doi:10.1016/0014-4827(61)90007-6.

Lew, D.J., and S.I. Reed. 1993. Morphogenesis in the yeast cell cycle: regulation by Cdc28 and cyclins. *J. Cell Biol.* 120:1305–1320. doi:10.1083/jcb.120.6.1305.

Lianga, N., E.C. Williams, E.K. Kennedy, C. Doré, S. Pilon, S.L. Girard, J.-S. Deneault, and A.D. Rudner. 2013. A Wee1 checkpoint inhibits anaphase onset. *J. Cell Biol.* 201:843–862. doi:10.1083/jcb.201212038.

Linkert, M., C.T. Rueden, C. Allan, J.-M. Burel, W. Moore, A. Patterson, B. Loranger, J. Moore, C. Neves, D. MacDonald, A. Tarkowska, C. Sticco, E. Hill, M. Rossner, K.W. Eliceiri, and J.R. Swedlow. 2010. Metadata matters: access to image data in the real world. *The Journal of Cell Biology*. 189:777–782. doi:10.1083/jcb.201004104.

Lippincott, J., and R. Li. 1998. Sequential assembly of myosin II, an IQGAP-like protein, and filamentous actin to a ring structure involved in budding yeast cytokinesis. *J. Cell Biol.* 140:355–366. doi:10.1083/jcb.140.2.355.

Longtine, M.S., A. McKenzie, D.J. Demarini, N.G. Shah, A. Wach, A. Brachat, P. Philippsen, and J.R. Pringle. 1998. Additional modules for versatile and economical PCR-based gene deletion and modification in Saccharomyces cerevisiae. *Yeast*. 14:953–961. doi:10.1002/(SICI)1097-0061(199807)14:10<953::AID-YEA293>3.0.CO;2-U.

Longtine, M.S., C.L. Theesfeld, J.N. McMillan, E. Weaver, J.R. Pringle, and D.J. Lew. 2000. Septin-dependent assembly of a cell cycle-regulatory module in Saccharomyces cerevisiae. *Mol. Cell. Biol.* 20:4049–4061.

Lorincz, A., and B.L.A. Carter. 1979. Control of cell size at bud initiation in Saccharomyces cerevisiae. *Microbiology*. doi:10.1099/00221287-113-2-287.

Ma, X.-J., Q. Lu, and M. Grunstein. 1996. A search for proteins that interact genetically with histone H3 and H4 amino termini uncovers novel regulators of the Swe1 kinase in Saccharomyces cerevisiae. *Genes & Development*. 10:1327–1340. doi:10.1101/gad.10.11.1327.

McCusker, D., C. Denison, S. Anderson, T.A. Egelhofer, J.R.I. Yates, S.P. Gygi, and D.R. Kellogg. 2007. Cdk1 coordinates cell-surface growth with the cell cycle. *Nat Cell Biol*. 9:506–U45. doi:10.1038/ncb1568.

McMillan, J.N., C.L. Theesfeld, J.C. Harrison, E.S.G. Bardes, and D.J. Lew. 2002. Determinants of Swe1p Degradation in Saccharomyces cerevisiae. *Molecular Biology of the Cell*. 13:3560–3575. doi:10.1091/mbc.E02.

McMillan, J.N., M.S. Longtine, R.A. Sia, C.L. Theesfeld, E.S. Bardes, J.R. Pringle, and D.J. Lew. 1999. The morphogenesis checkpoint in Saccharomyces cerevisiae: cell cycle control of Swe1p degradation by Hsl1p and Hsl7p. *Mol. Cell. Biol.* 19:6929–6939.

Mitchison, J.M. 1958. The growth of single cells. II. Saccharomyces cerevisiae. *Exp. Cell Res.* 15:214–221.

Nash, R., G. Tokiwa, S. Anand, K. Erickson, and A.B. Futcher. 1988. The WHI1+ gene of Saccharomyces cerevisiae tethers cell division to cell size and is a cyclin homolog. *EMBO J.* 7:4335–4346.

Nishimura, K., T. Fukagawa, H. Takisawa, T. Kakimoto, and M. Kanemaki. 2009. An auxin-based degron system for the rapid depletion of proteins in nonplant cells. *Nature Methods*. 6:917–922. doi:10.1038/nmeth.1401.

Nurse, P. 1975. Genetic control of cell size at cell division in yeast. *Nature*. 256:547–551. doi:10.1038/256547a0.

Pringle, J.R., A.E.M. Adams, D.G. Drubin, and B.K. Haarer. 1991. Immunofluorescence methods for yeast. *In* Methods in Enzymology. Academic Press. 565–602.

Raspelli, E., C. Cassani, E. Chiroli, and R. Fraschini. 2014. Budding Yeast Swe1 is Involved in the Control of Mitotic Spindle Elongation and is Regulated by Cdc14 Phosphatase during Mitosis. *Journal of Biological Chemistry*. jbc.M114.590984. doi:10.1074/jbc.M114.590984.

Raspelli, E., C. Cassani, G. Lucchini, and R. Fraschini. 2011. Budding yeast Dma1 and Dma2 participate in regulation of Swe1 levels and localization. *Molecular Biology of the Cell*. 22:2185–2197. doi:10.1091/mbc.E11-02-0127.

Richardson, H.E., C. Wittenberg, F. Cross, and S.I. Reed. 1989. An essential G1 function for cyclin-like proteins in yeast. *Cell*. 59:1127–1133. doi:10.1016/0092-8674(89)90768-X.

RStudio Team. 2015. RStudio: Integrated Development Environment for R. http://www.rstudio.com.

Schmoller, K.M., J.J. Turner, M. Kõivomägi, and J.M. Skotheim. 2015. Dilution of the cell cycle inhibitor Whi5 controls budding-yeast cell size. *Nature*. 526:268–272. doi:10.1038/nature14908.

Schneider, C.A., W.S. Rasband, and K.W. Eliceiri. 2012. NIH Image to ImageJ: 25 years of image analysis. *Nature Methods*. 9:671–675.

Sreenivasan, A., and D.R. Kellogg. 1999. The Elm1 Kinase Functions in a Mitotic Signaling Network in Budding Yeast. *Mol. Cell. Biol.* 19:7983–7994. doi:10.1128/MCB.19.12.7983.

Su, S.S., Y. Tanaka, I. Samejima, K. Tanaka, and M. Yanagida. 1996. A nitrogen starvation-induced dormant G0 state in fission yeast: the establishment from uncommitted G1 state and its delay for return to proliferation. *J Cell Sci*. 109:1347–1357.

The R Core Team. 2016. R: A language and environment for statistical computing.

Thevenaz, P., U.E. Ruttimann, and M. Unser. 1998. A pyramid approach to subpixel registration based on intensity. *IEEE Transactions on Image Processing*. 7:27–41. doi:10.1109/83.650848.

Tinker-Kulberg, R.L., and D.O. Morgan. 1999. Pds1 and Esp1 control both anaphase and mitotic exit in normal cells and after DNA damage. *Genes & Development*. 13:1936–1949.

Toledo, C.M., Y. Ding, P. Hoellerbauer, R.J. Davis, R. Basom, E.J. Girard, E. Lee, P. Corrin, T. Hart, H. Bolouri, J. Davison, Q. Zhang, J. Hardcastle, B.J. Aronow, C.L. Plaisier, N.S. Baliga, J. Moffat, Q. Lin, X.-N. Li, D.-H. Nam, J. Lee, S.M. Pollard, J. Zhu, J.J. Delrow, B.E. Clurman, J.M. Olson, and P.J. Paddison. 2015. Genome-wide CRISPR-Cas9 Screens Reveal Loss of Redundancy between PKMYT1 and WEE1 in Glioblastoma Stem-like Cells. *CellReports*. 13:1–16. doi:10.1016/j.celrep.2015.11.021.

Tseng, Q. Find Focused Slices. https://sites.google.com/site/qingzongtseng/find-focus.

Wang, H., D. Liu, Y. Wang, J. Qin, and S.J. Elledge. 2001. Pds1 phosphorylation in response to DNA damage is essential for its DNA damage checkpoint function. *Genes & Development*. 15:1361–1372. doi:10.1101/gad.893201.

Weisz, P.B. 1954. Morphogenesis in Protozoa. *Q Rev Biol*. 29:207–229.

Wickham, H. 2009. ggplot2: Elegant Graphics for Data Analysis. Springer-Verlag, New York.

Winey, M., and E. O'Toole. 2001. The spindle cycle in budding yeast. *Nat Cell Biol*. 3:E23–E27. doi:10.1038/35050663.

Wood, E., and P. Nurse. 2013. Pom1 and cell size homeostasis in fission yeast. *Cell Cycle*. 12:3228–3236. doi:10.4161/cc.26462.

Yamamoto, A., V. Guacci, and D. Koshland. 1996. Pds1p is required for faithful execution of anaphase in the yeast, Saccharomyces cerevisiae. *J. Cell Biol.* 133:85–97. doi:10.1083/jcb.133.1.85.

Young, P.G., and P.A. Fantes. 1987. Schizosaccharomyces pombe mutants affected in their division response to starvation. *J Cell Sci*. 88:295–304.

Zapata, J., N.E. Dephoure, T. MacDonough, Y. Yu, E.J. Parnell, M. Mooring, S.P. Gygi, D.J. Stillman, and D.R. Kellogg. 2014. PP2ARts1 is a master regulator of pathways that control cell size. *J. Cell Biol.* 204:359–376. doi:10.1083/jcb.201309119.

Figure Legends

Figure 1. **The duration of mitosis is modulated by nutrients.** (**A**) Wild type cells growing in YPD (rich carbon) or YPGE (poor carbon) were arrested in G1 phase by addition of mating pheromone. The cells were released from the arrest and levels of the mitotic cyclin Clb2 were assayed by western blot. (**B,C**) Cells growing in YPD were released from a G1 arrest. At 90 minutes, the culture was split and one half was washed into YPD and the other half was washed into YPGE. Levels of the mitotic cyclin Clb2 were assayed by western blot and short metaphase spindles were assayed by immunofluorescence. (**D,E**) Cells growing in YPD were released from a G1 arrest. At 105 minutes, the culture was split and one half was washed into YPD the other half was washed into YPGE. Levels of the mitotic cyclin Clb2 were assayed by western blot and long anaphase spindles were assayed by immunofluorescence.

Figure 2. **Simultaneous imaging of bud growth and mitotic spindle dynamics in living single cells.** (**A,B**) Representative growth curves for cells growing in rich carbon (**A**) or poor carbon (**B**). The volume of the daughter bud is plotted in blue and the distance between spindle poles in green. (**C**) Contrast enhanced images of a representative growing bud with GFP tagged spindle poles (Spc42-GFP) and myosin ring (Myo1-GFP). Key transitions are highlighted. Images taken in metaphase that were omitted so that all key transition points could be shown are indicate with ▪▪▪ .

Figure 3. The duration of mitosis and bud volume are modulated by nutrients. (**A**) A plot showing the average durations of metaphase and anaphase for cells growing in rich or poor carbon. (**B**) A plot showing the average durations of all cell cycle stages for cells growing in rich or poor carbon. (**C**) A plot showing the average growth in volume during all phases of the cell cycle for cells growing in rich or poor carbon. Error bars represent standard error of the mean.

Figure 4. Growth rate changes during the cell cycle and is modulated by nutrients.
The growth rate at each phase of the cell cycle was calculated as the average of individual cell growth rates during each cell cycle phase. The growth rate of each cell was calculated by dividing the volume increase of the cell during a phase by the time the cell spent in the phase. (**A**) Data for cells growing in rich carbon. (**B**) Data for cells growing in poor carbon. Error bars represent the standard error of the mean.

Figure 5. The growth rate and final volume of a daughter bud is influenced by the size of its mother cell. (**A**) The growth rate in mitosis of each daughter bud was plotted against the volume of its mother cell. (**B**) The volume of each daughter bud at cytokinesis was plotted against the size of its mother. Red dots represent cells in rich carbon. Blue dots represent cells in poor carbon. Smooth lines are logistic regressions of the data. Shaded areas represent 95% confidence interval.

Figure 6. Cell size at cytokinesis is proportional to the growth rate during mitosis. The volume of daughter cells at cytokinesis was plotted against their growth rate during mitosis. Red dots represent cells in rich carbon. Blue dots represent cells in poor carbon. Smooth lines are logistic regressions of the data. Shaded areas represent 95% confidence interval.

Figure 7. $PP2A^{Rts1}$ is required for normal control of mitotic duration and cell size. (**A,B**) Plots showing the average durations of metaphase and anaphase for wild type and *rts1-AID* cells grown in rich or poor carbon. (**C,D**) The average growth in volume for all phases of the cell cycle except G1 is plotted for wild type and *rts1-AID* cells grown in rich or poor carbon. Due to the extended length of the cell cycle in *rts1-AID* cells, only a few cells were followed through G1.

For this reason, we omitted the limited data regarding G1 from these plots. (**E**) The growth rate during metaphase and anaphase was calculated as the average of individual cell growth rates. The growth rate of each cell was calculated by dividing its volume increase during metaphase and anaphase by the time it spent in these phases. (**F**) The volume of the daughter bud at completion of anaphase is plotted as a function of growth rate during metaphase plus anaphase. For panels C and D, red and blue represent wild type cells in rich and poor carbon, respectively. Similarly, yellow and green represents *rts1-AID* cells in rich and poor carbon. Error bars represent standard error of the mean.

Figure 8. The increased duration of mitosis in poor carbon is partially due to Cdk1 inhibitory phosphorylation. (**A,B**) The same samples used for figure 1A were probed for Cdk1-Y19 phosphorylation (**A**) and Swe1 (**B**) by western blot.

Figure 9. The increased duration of mitosis in poor carbon is partially due to Cdk1 inhibitory phosphorylation. (**A**) A plot showing the average durations of metaphase and anaphase for wild type and *swe1*Δ cells growing in rich carbon. (**B**) A plot showing the average durations of metaphase and anaphase for wild type and *swe1*Δ cells growing in poor carbon. (**C**) A plot showing the average growth rate during metaphase and anaphase in wild type or *swe1*Δ cells in rich or poor carbon. (**D**) A plot showing the average growth in volume during metaphase and anaphase for wild type or *swe1*Δ cells growing in rich carbon. (**E**) A plot showing the average growth in volume during metaphase and anaphase for wild type or *swe1*Δ cells growing in poor carbon. Error bars represent standard error of the mean.

Figure 10. $PP2A^{Rts1}$ controls the duration of mitosis by Swe1-dependent and Swe1-independent mechanisms. (**A**) Cells of the indicated genotypes, grown in YPD or YPGE, were released from a G1 arrest and auxin was added at 45 min (YPD) or 75min (YPGE). Addition of auxin is denoted by *. Levels of the mitotic cyclin Clb2 were assayed by western blot. (**B**) Cells of the indicated genotypes were arrested in metaphase by depletion of Cdc20. After release from the arrest, levels of the mitotic cyclin Clb2 were assayed by western blot.

Figure 11. $PP2A^{Rts1}$ controls the duration of mitosis by Swe1-dependent and Swe1-independent mechanisms. (**A**) A plot showing the average durations of metaphase and anaphase for cells of the indicated genotypes growing in rich carbon. (**B**) A plot showing the average durations of metaphase and anaphase for cells of the indicated genotypes growing in poor carbon. (**C**) A plot showing the average growth in volume during metaphase and anaphase for cells of the indicated genotypes growing in rich carbon. (**D**) A plot showing the average growth in volume during metaphase and anaphase for cells of the indicated genotypes growing in poor carbon. (**E**) A plot showing the average growth rate during metaphase and anaphase in wild type or *swe1*Δ cells in rich or poor carbon. Error bars represent standard error of the mean.

Figure 1

The duration of mitosis is modulated by nutrients.

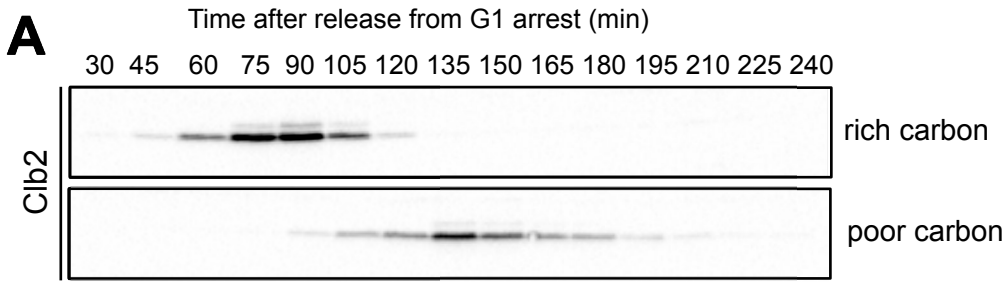

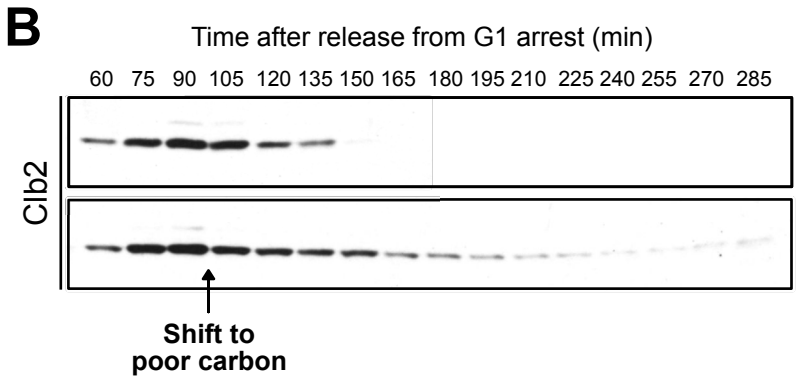

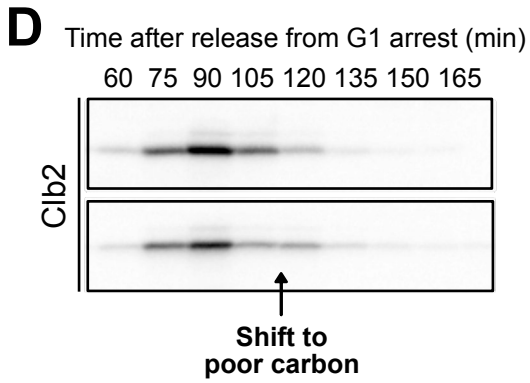

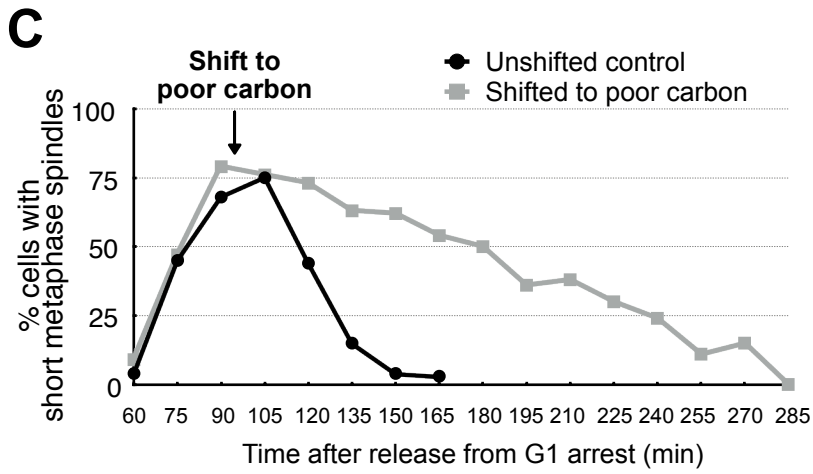

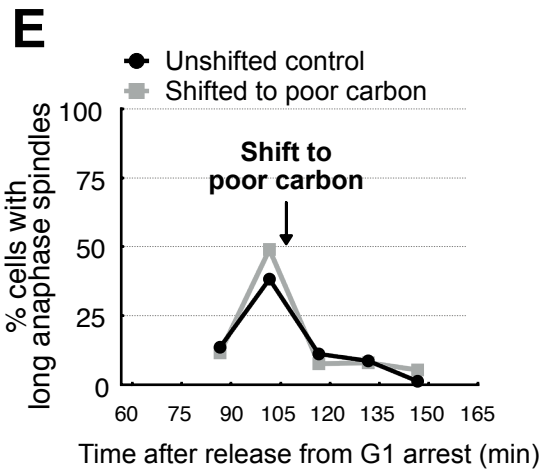

Figure 2

Simultaneous imaging of bud growth and mitotic spindle dynamics in living single cells

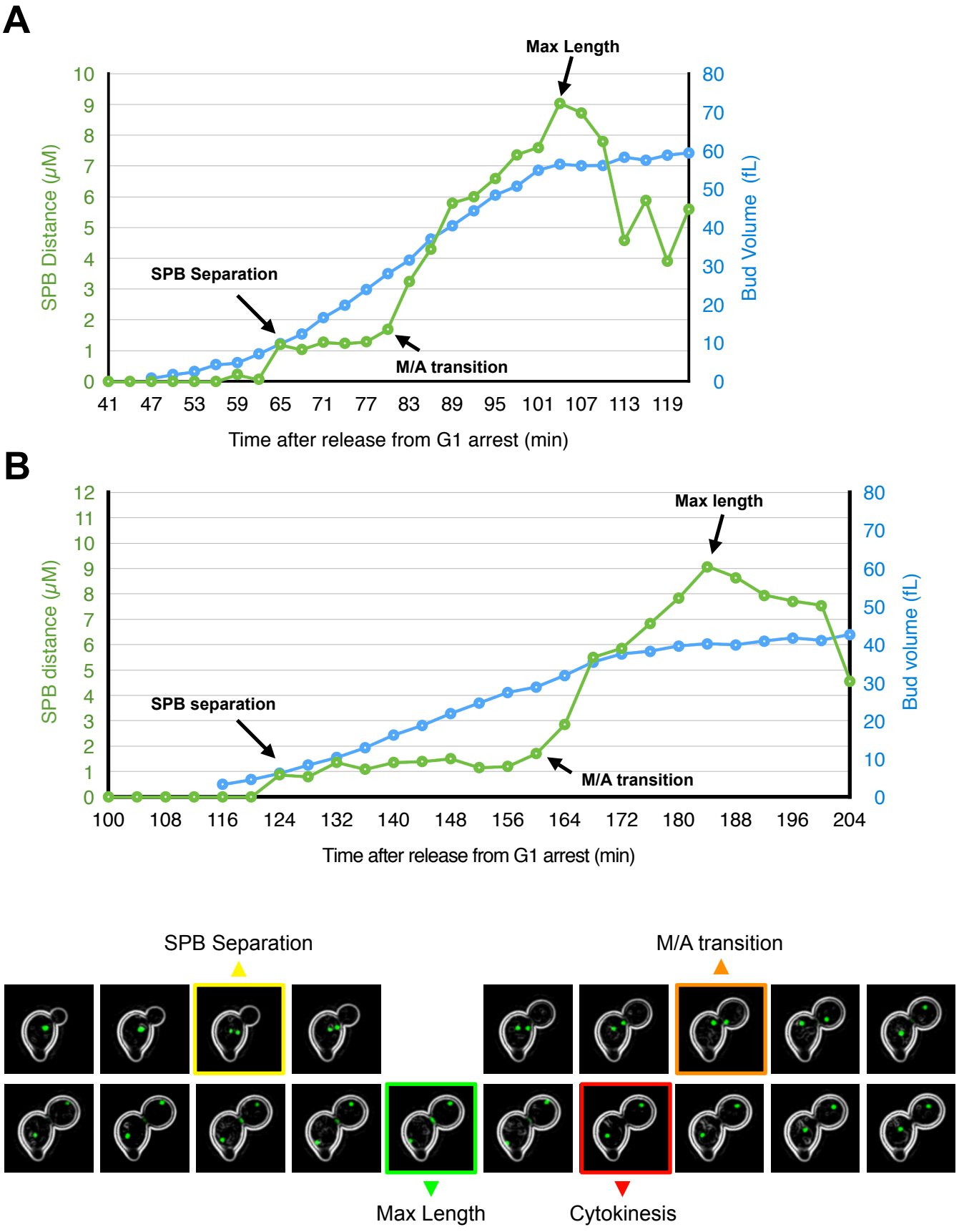

Figure 3

The duration of mitosis and bud volume are modulated by nutrients

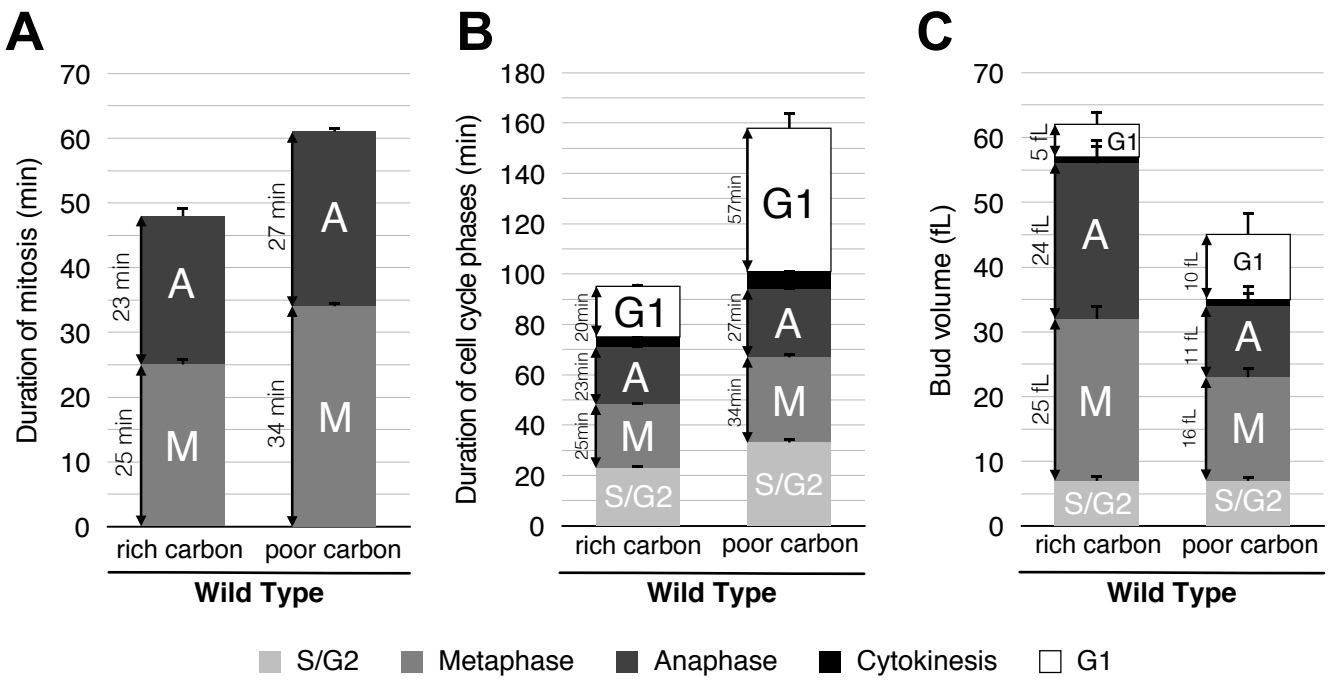

Figure 4

Growth rate changes during the cell cycle and is modulated by nutrients

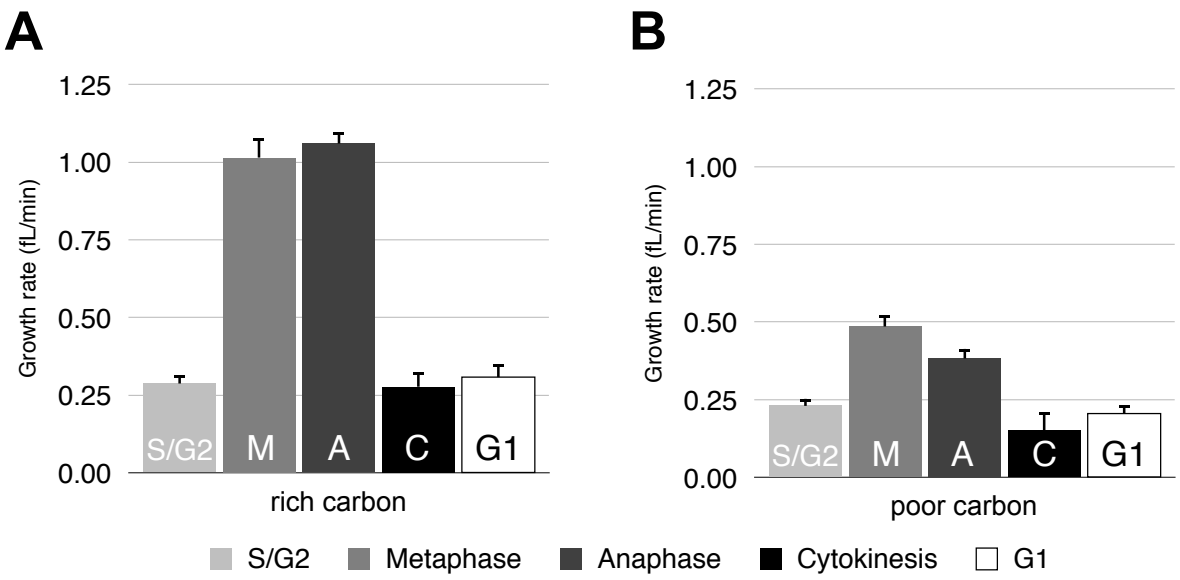

Figure 5

The growth rate and final volume of a daughter bud is influenced by the size of its mother cell

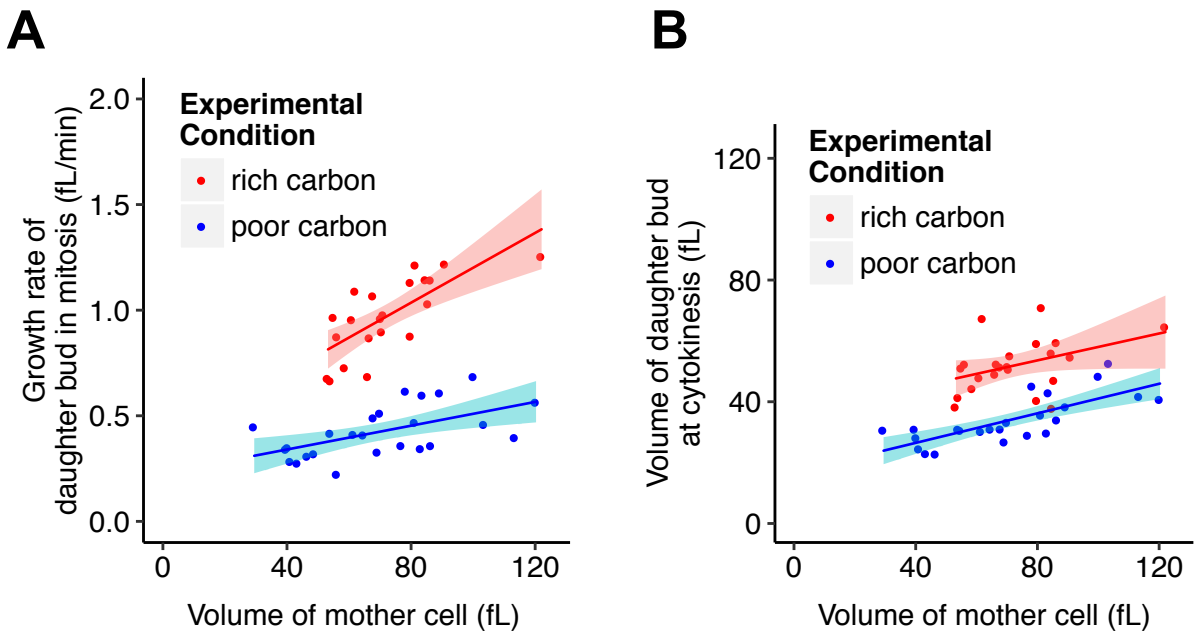

Figure 6

Cell size at completion of cytokinesis is proportional to the growth rate during mitosis

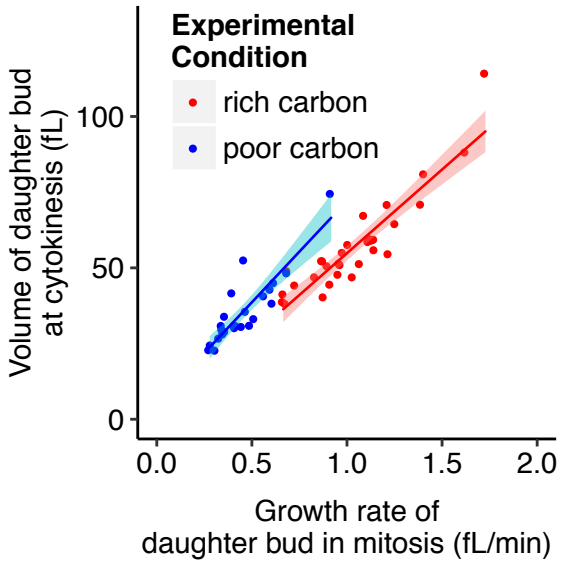

Figure 7

PP2A^{Rts1} is required for normal control of mitotic duration and cell size

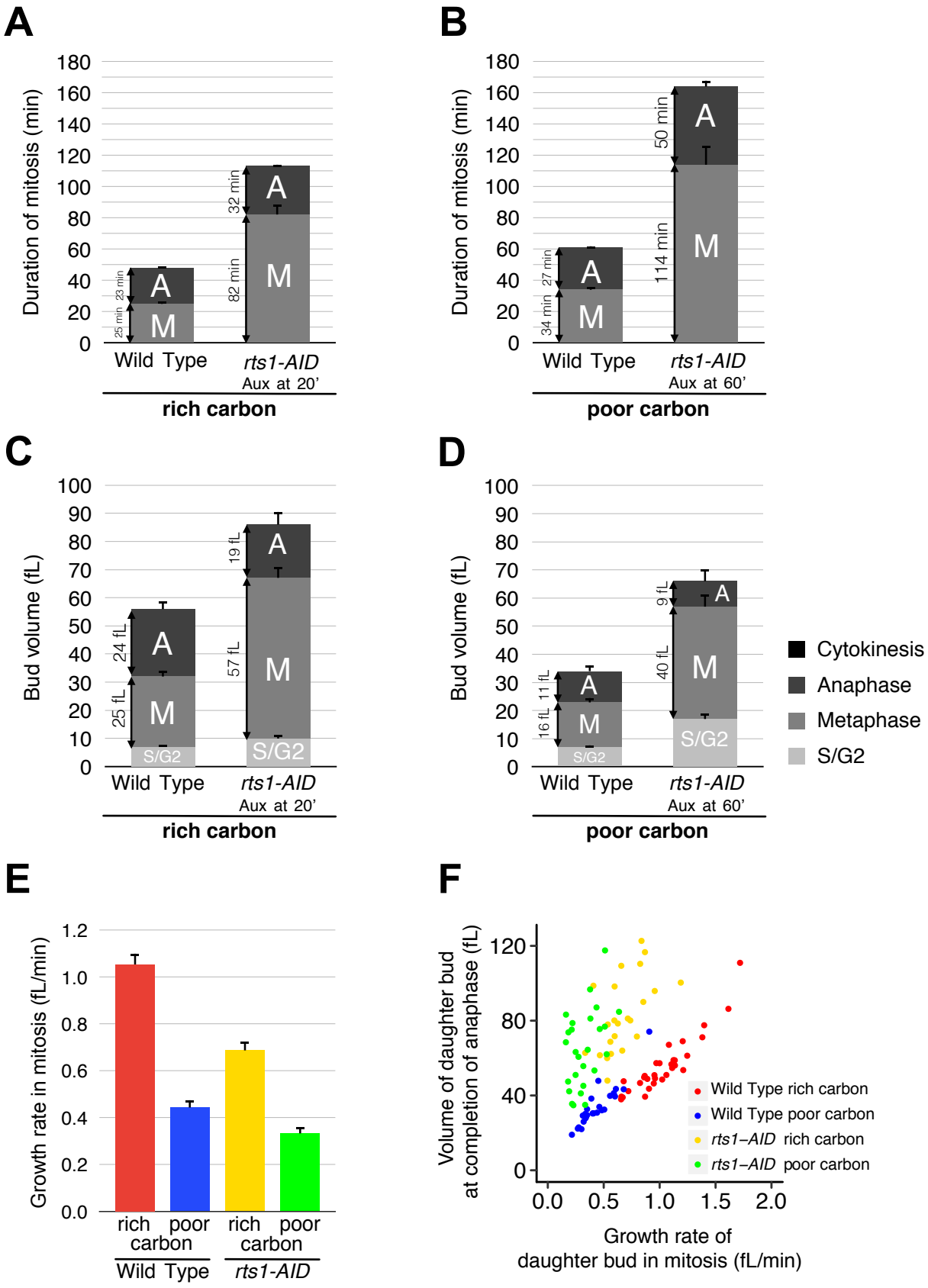

Figure 8

The increased duration of mitosis in poor carbon is partially due to Cdk1 inhibitory phosphorylation

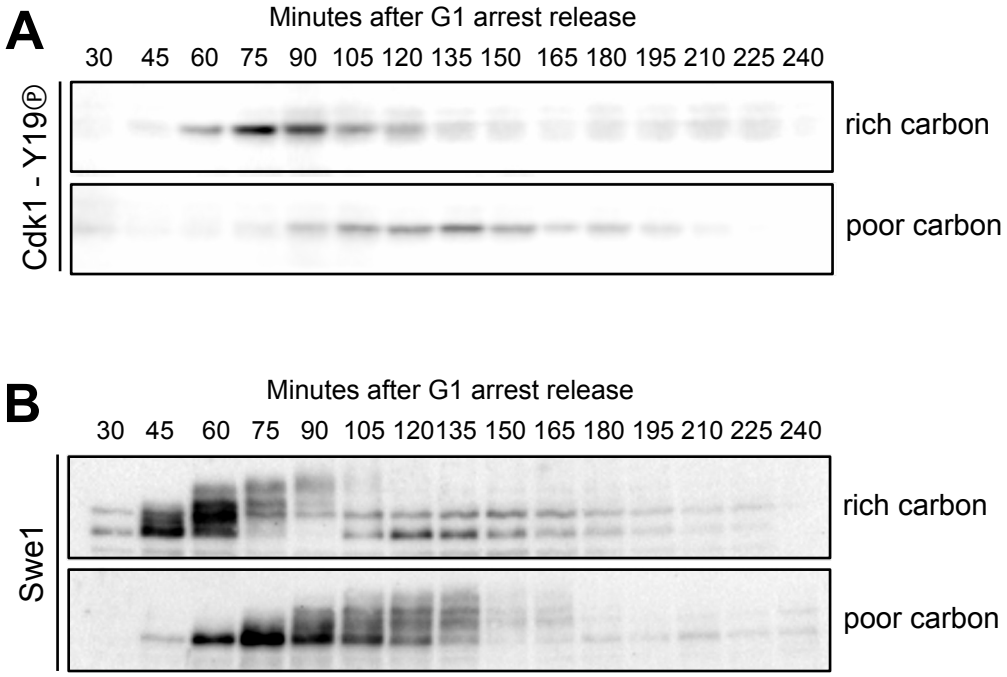

Figure 9

The increased duration of mitosis in poor carbon is partially due to Cdk1 inhibitory phosphorylation

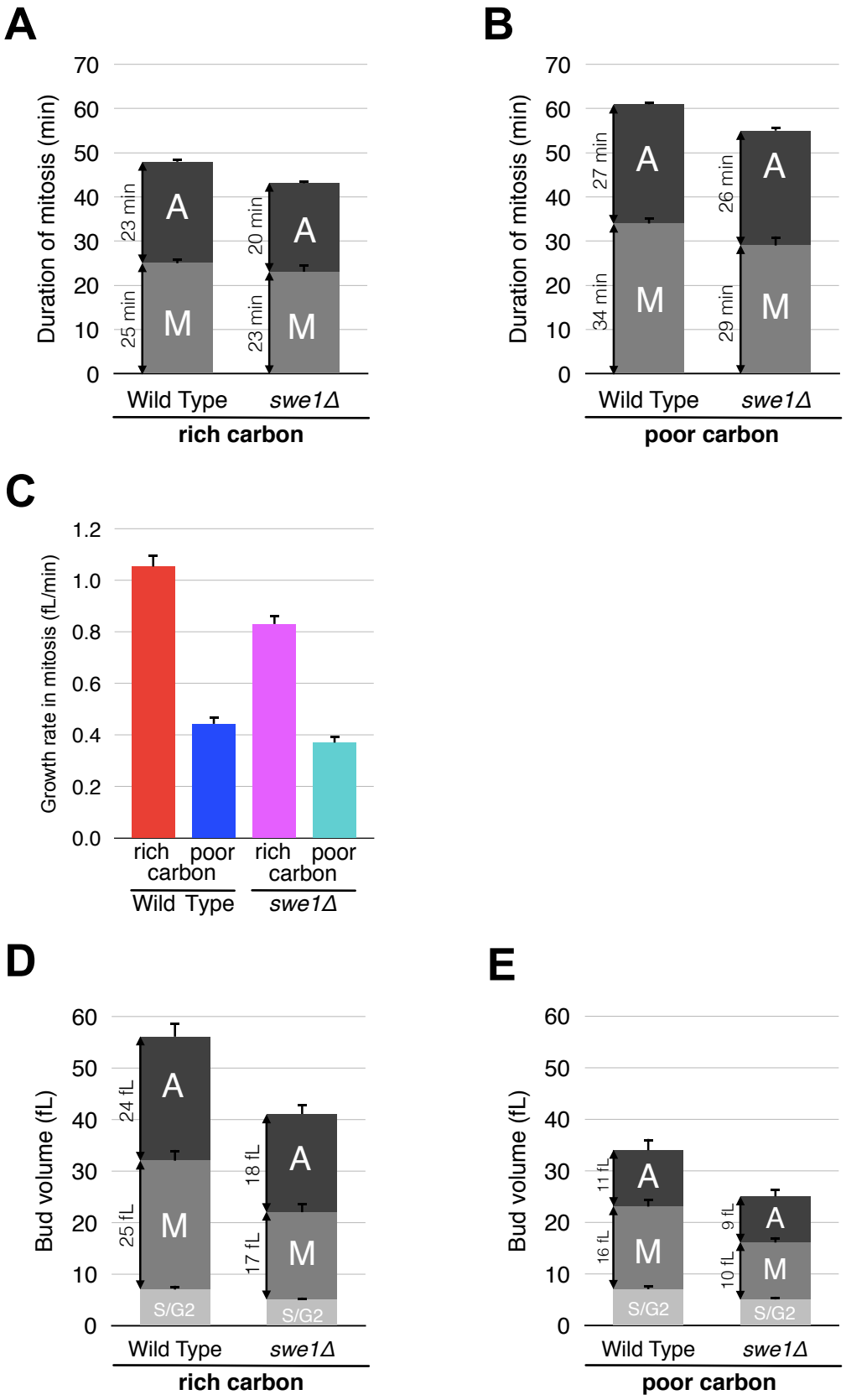

Figure 10

PP2A^{Rts1} controls the duration of mitosis by Swe1-dependent and Swe1-independent mechanisms

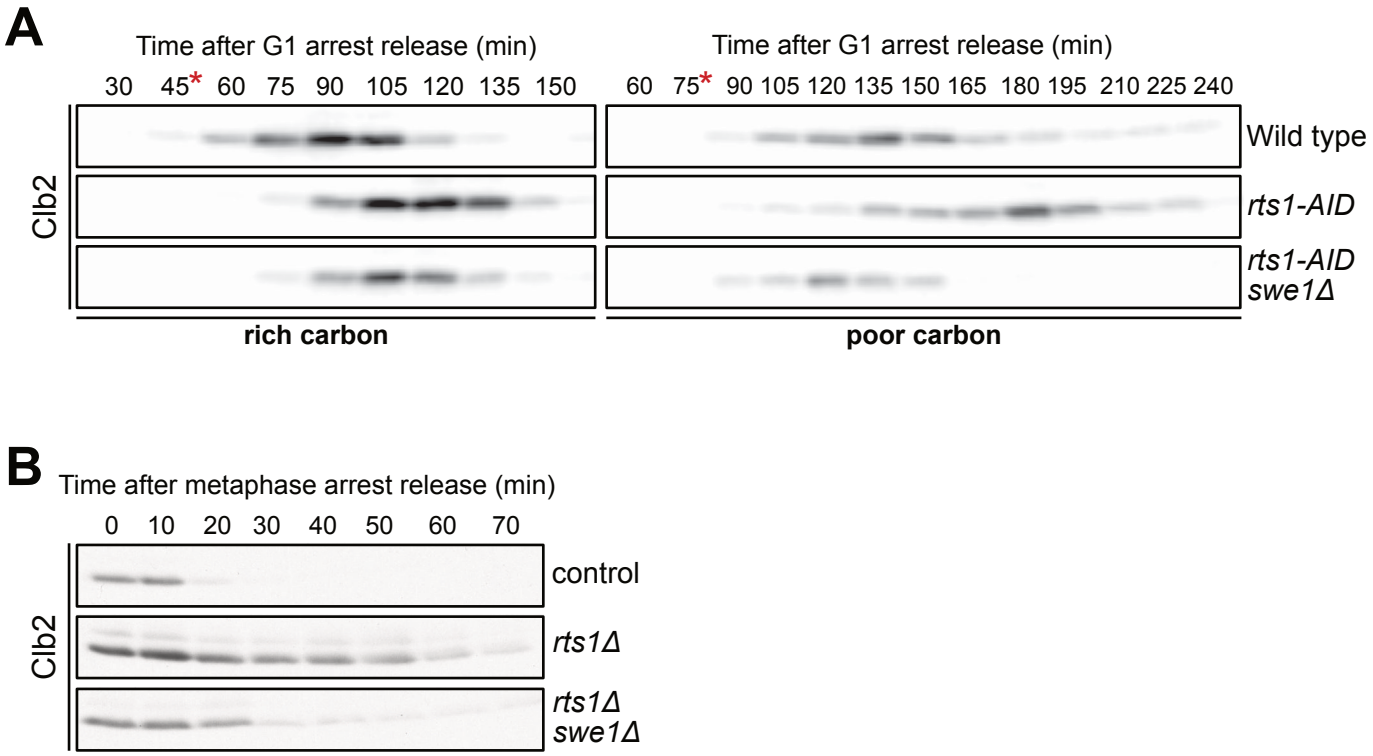

Figure 11

PP2A^{Rts1} controls the duration of mitosis by Swe1-dependent and Swe1-independent mechanisms

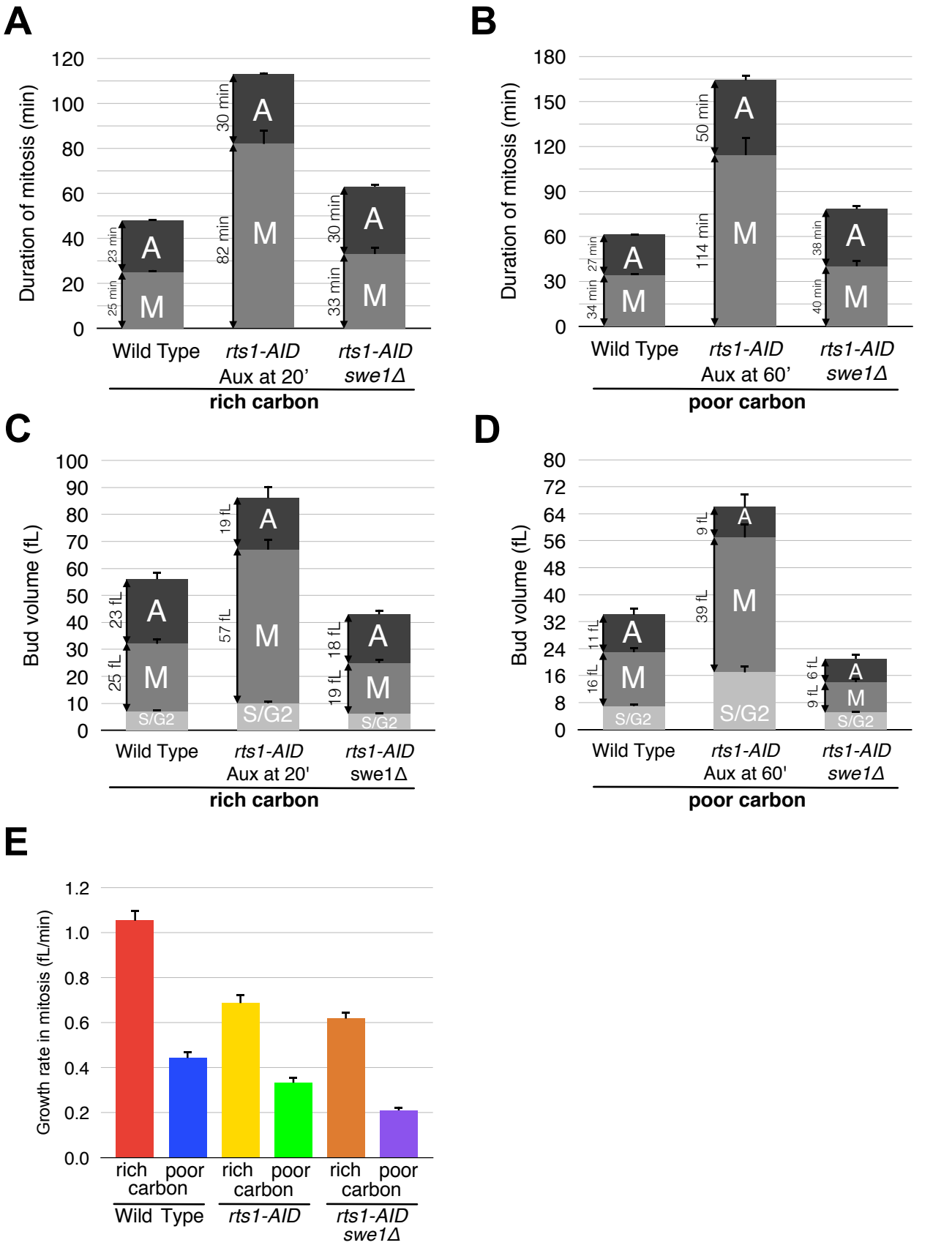

Figure S1

Growth curves for cells growing in rich carbon

A

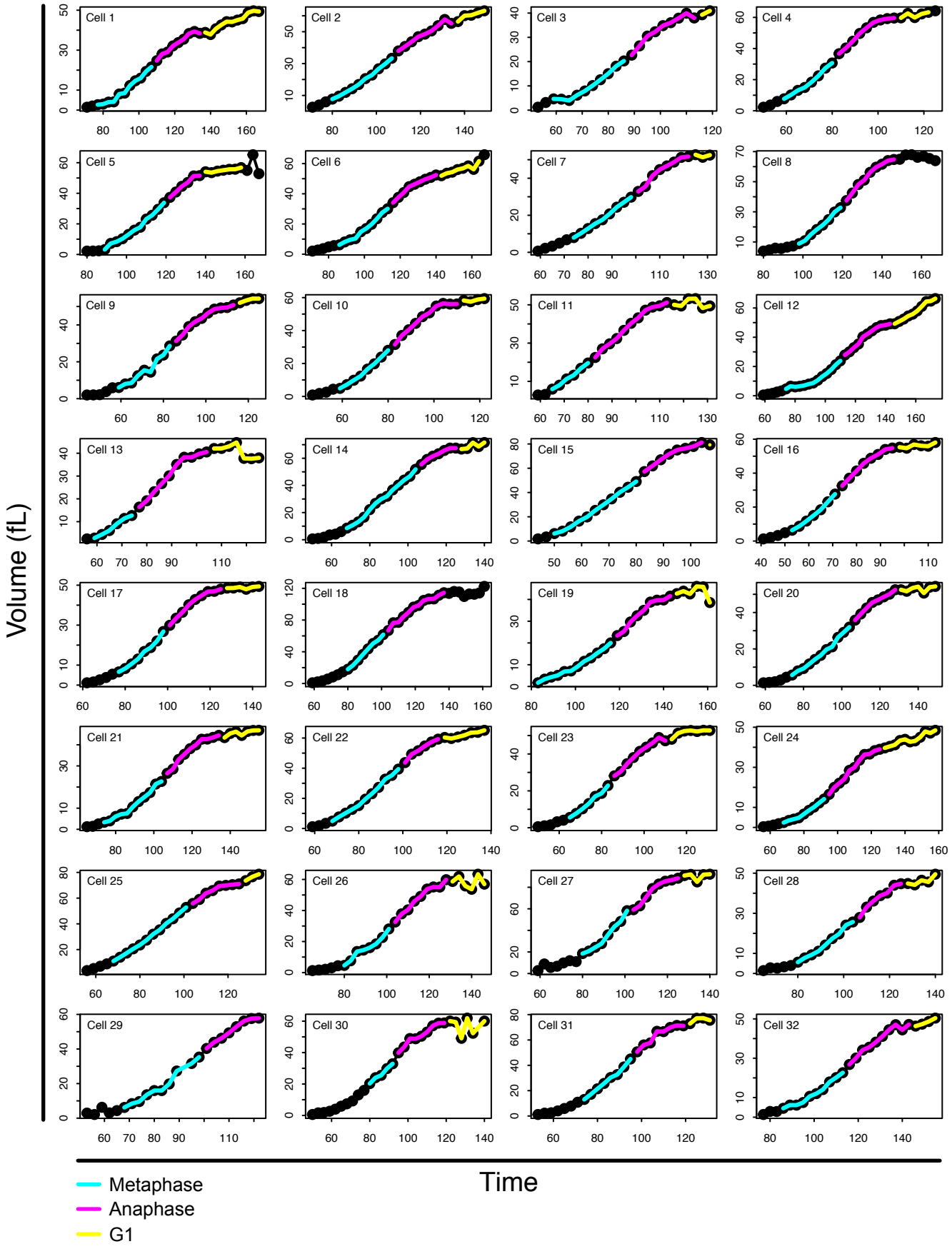

Figure S1B

Growth curves for yeast cells growing in poor carbon

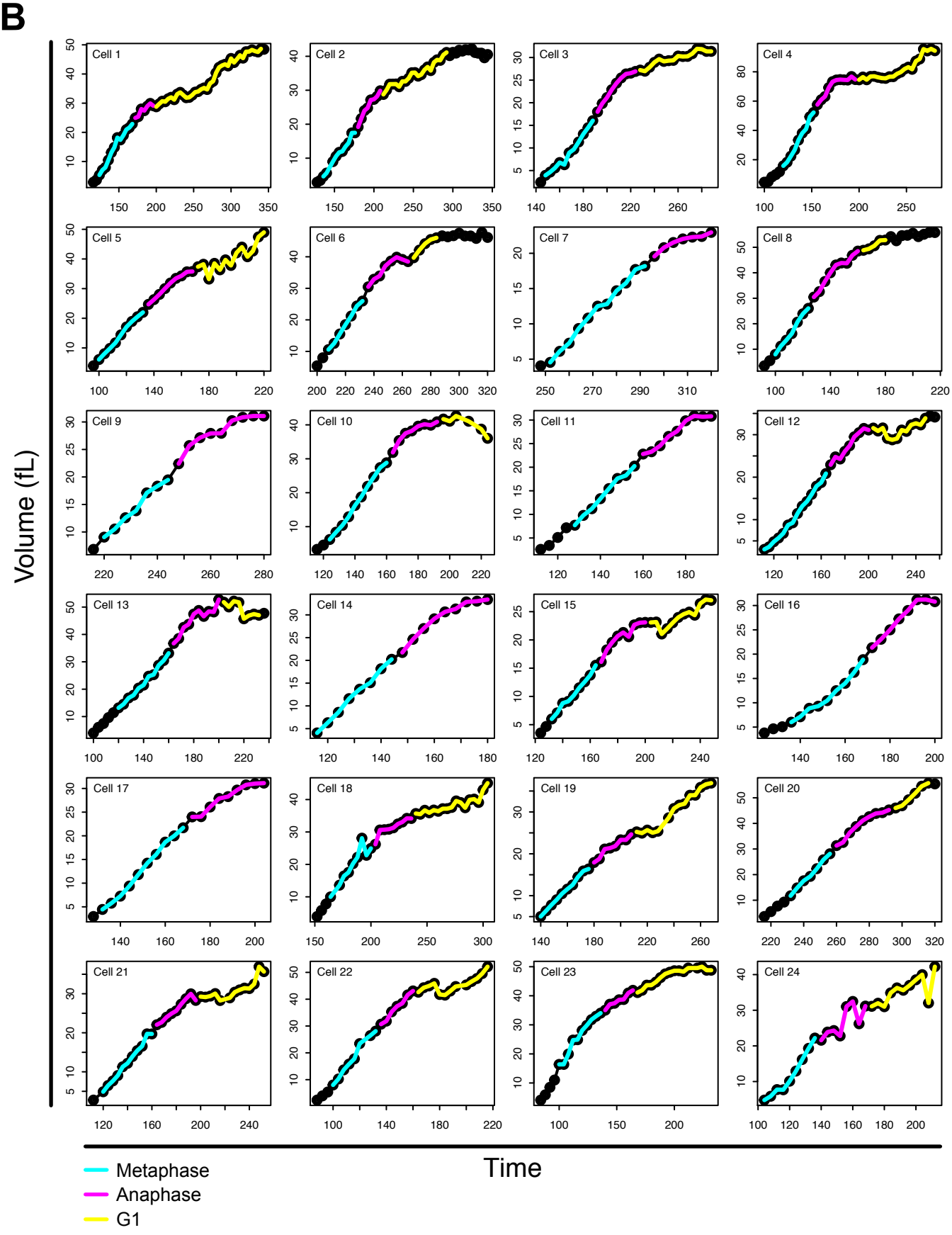

Figure S2

Dot plot versions of the data used to generate Figures 3A,B

A

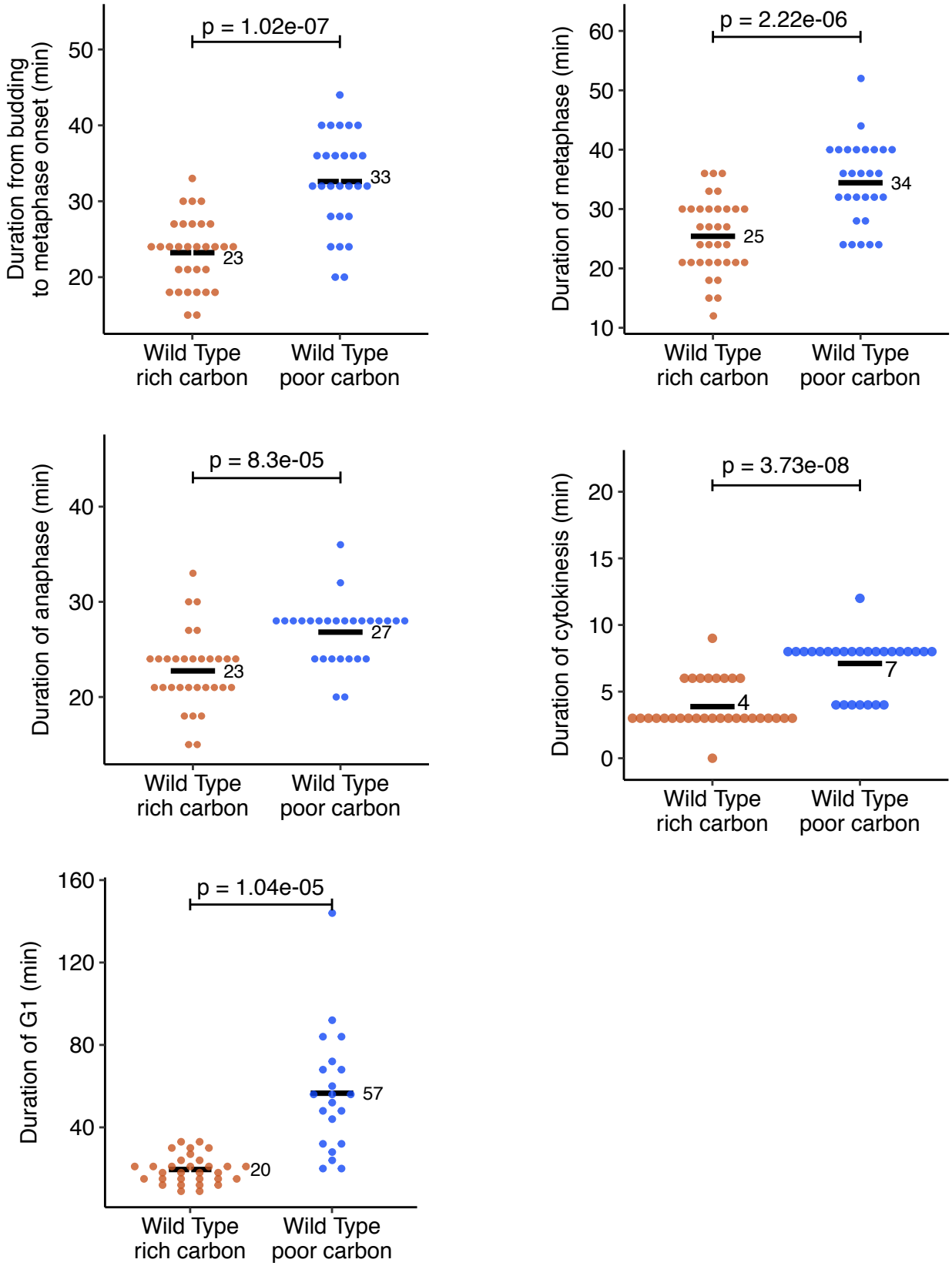

Figure S2

Dot plot versions of the data used to generate Figure 3C

B

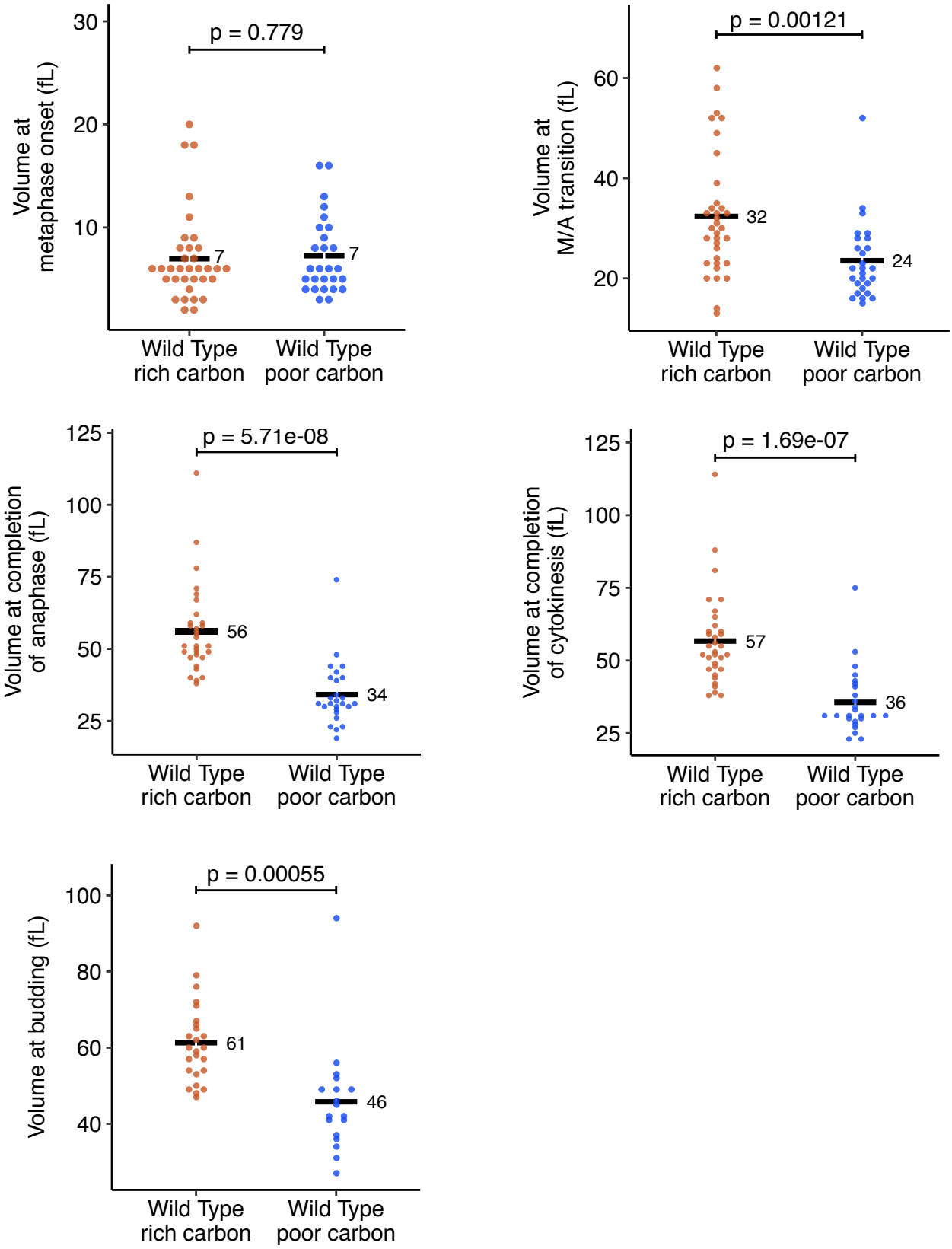

Figure S3

Characterization of rts1-AID cells

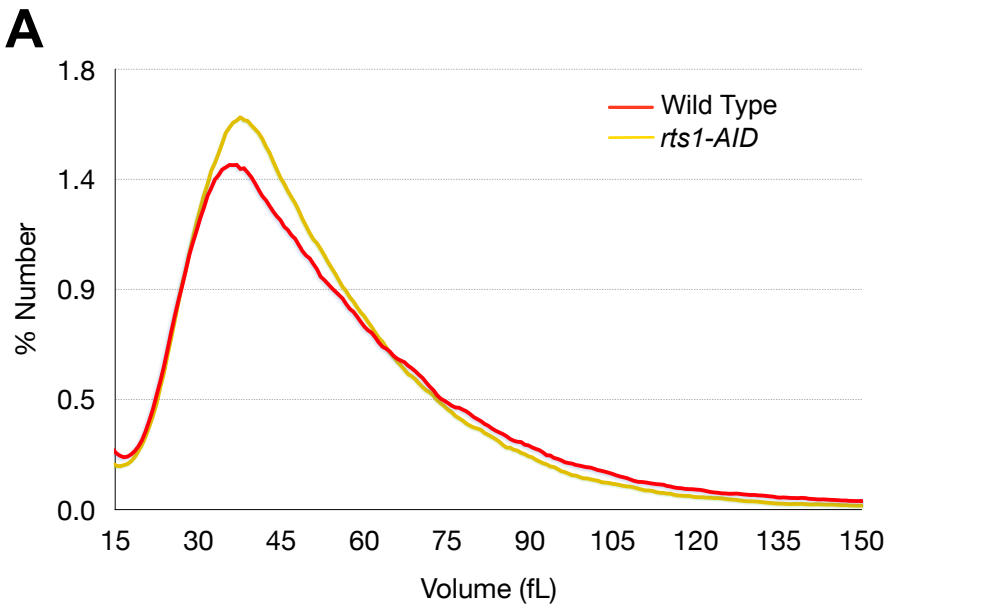

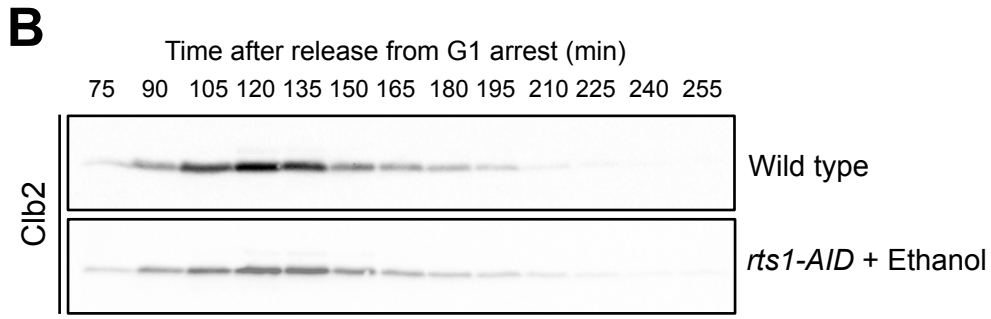

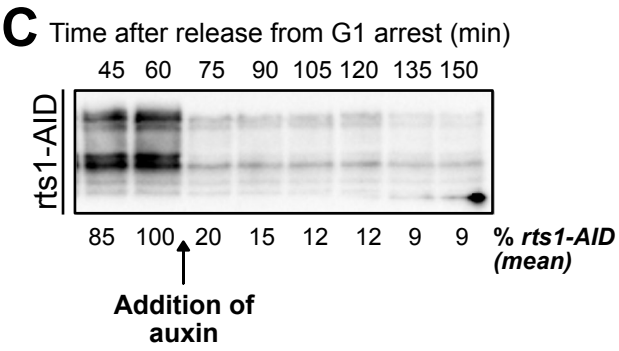

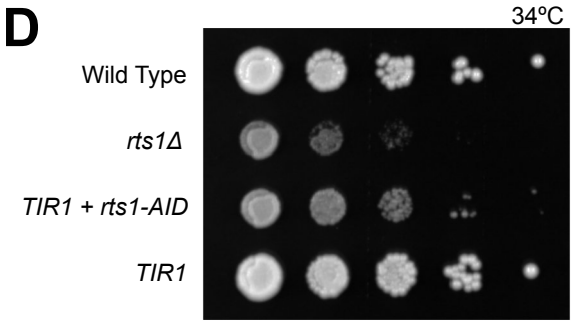

Figure S4

Dot plot versions of the data used to generate Figures 7A,B

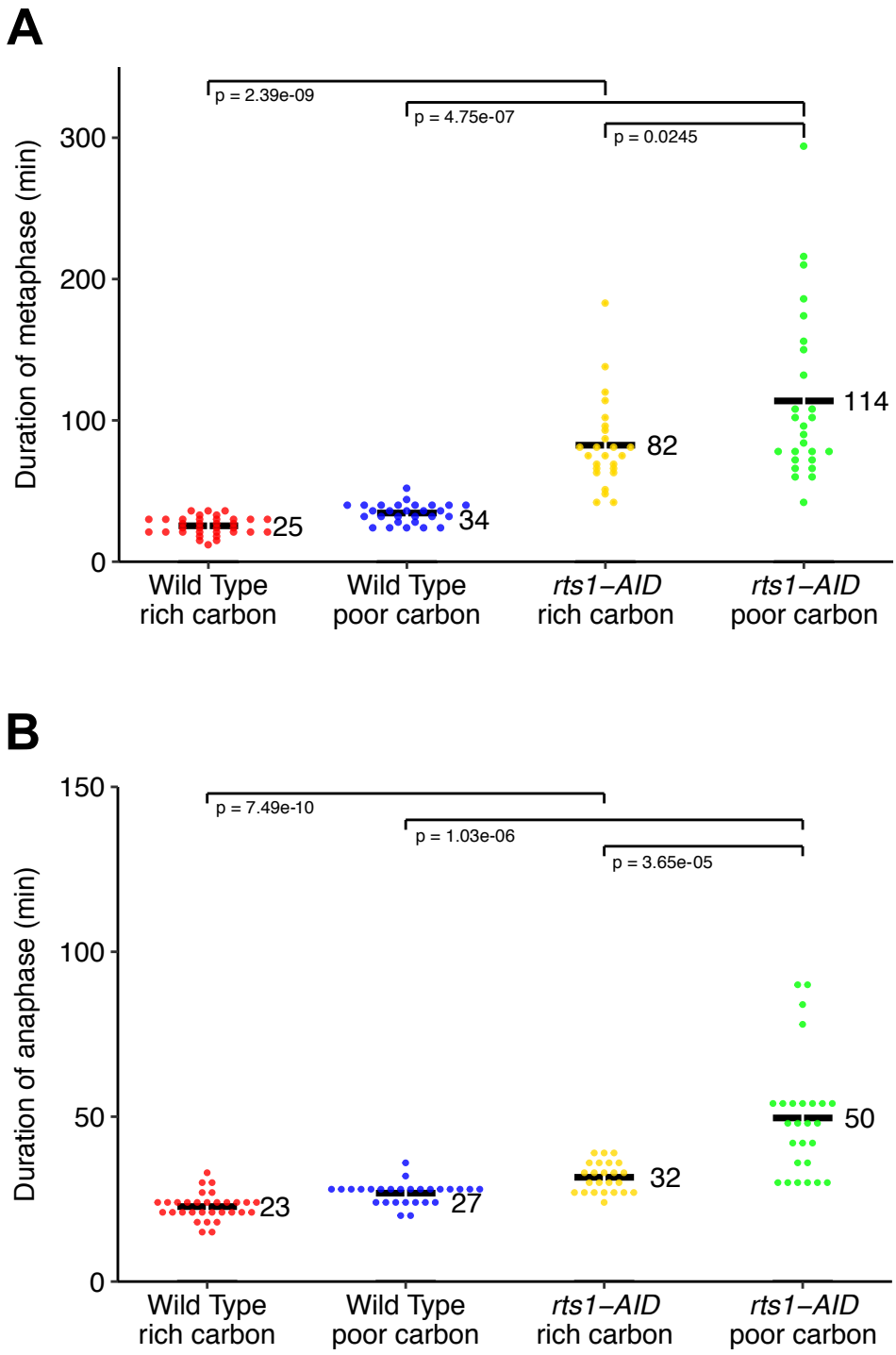

Figure S4

Dot plot versions of the data used to generate Figures 7C,D

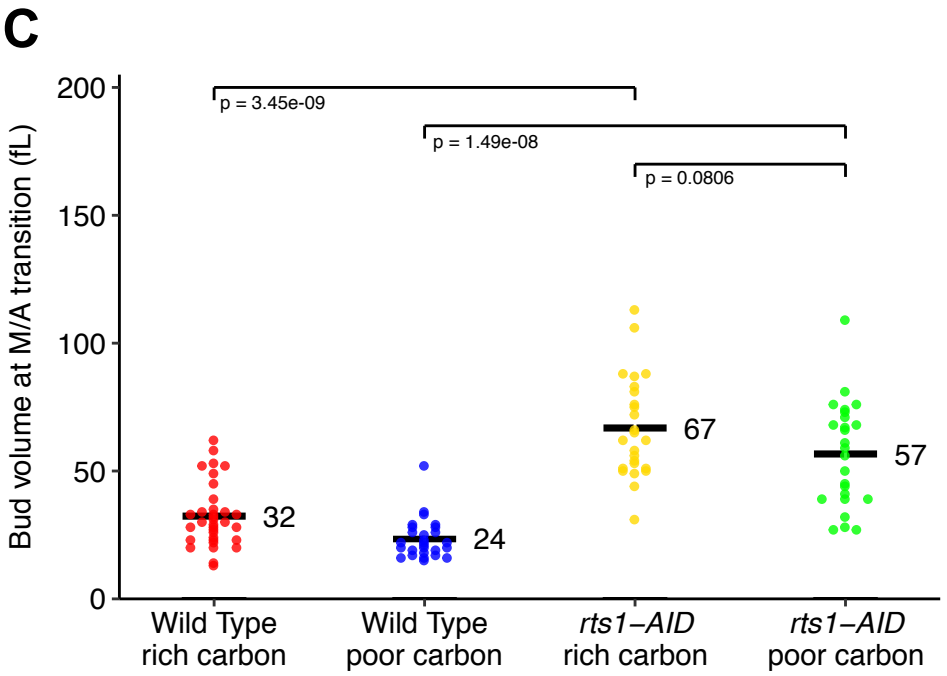

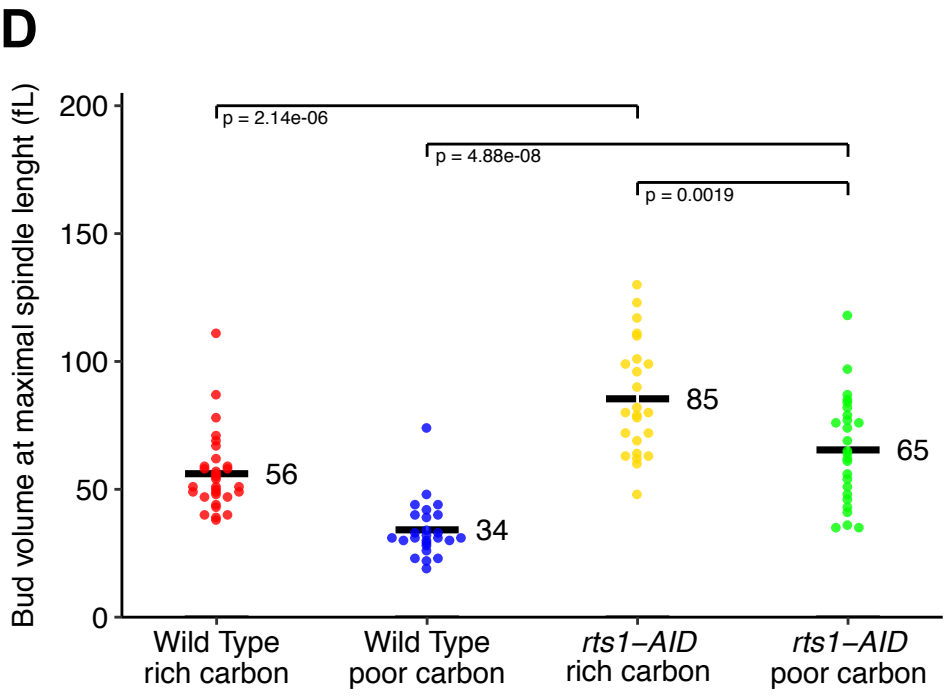

Figure S4

Dot plot versions of the data used to generate Figure 7E

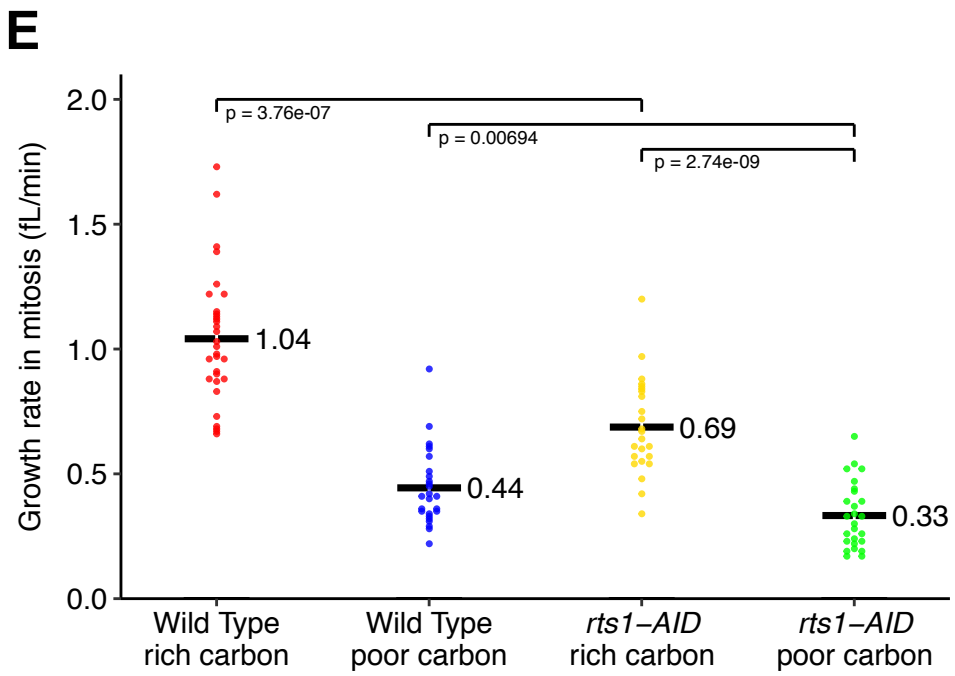

Figure S5

Dot plot versions of the data used to generate Figures 9A,B

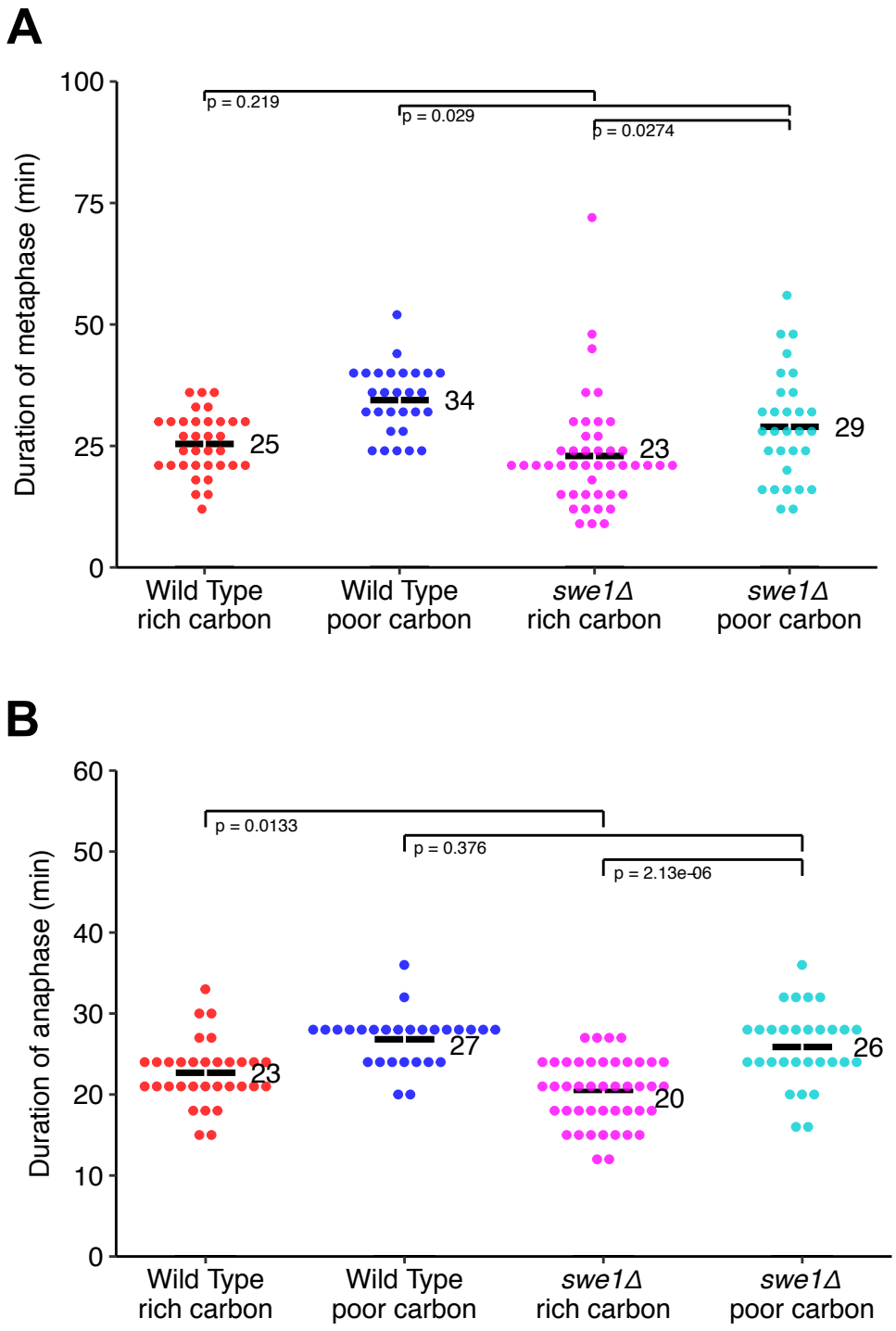

Figure S5

Dot plot versions of the data used to generate Figures 9D,E

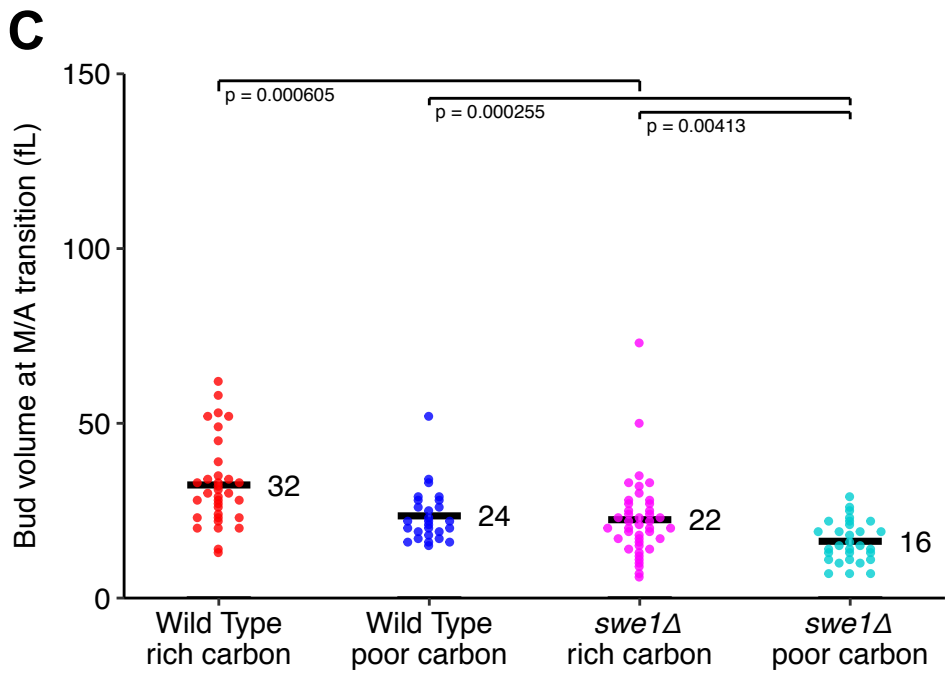

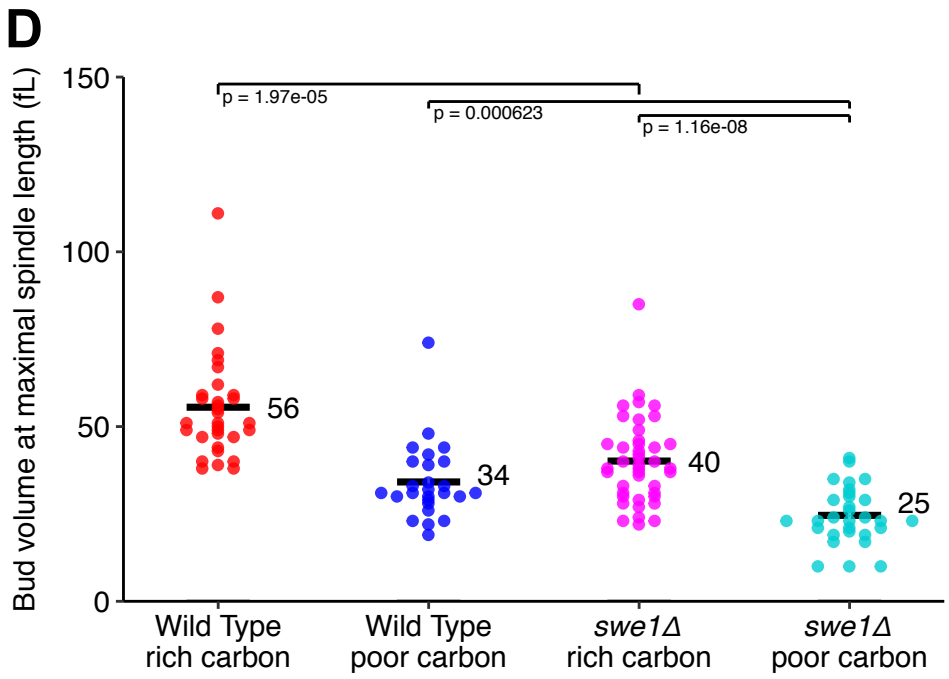

Figure S5

Dot plot versions of the data used to generate Figures 11A,B

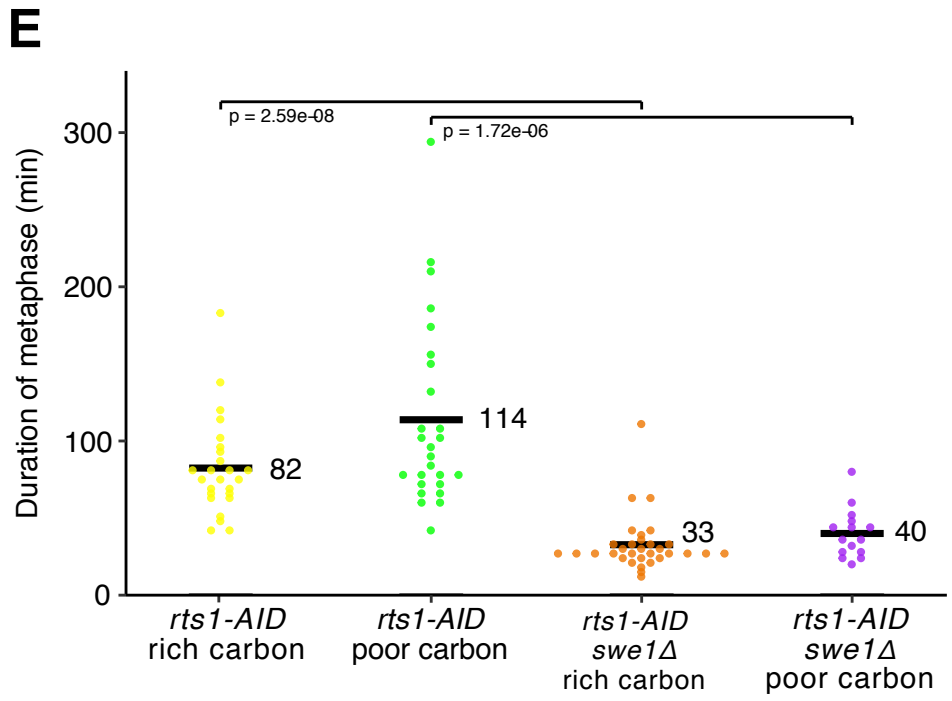

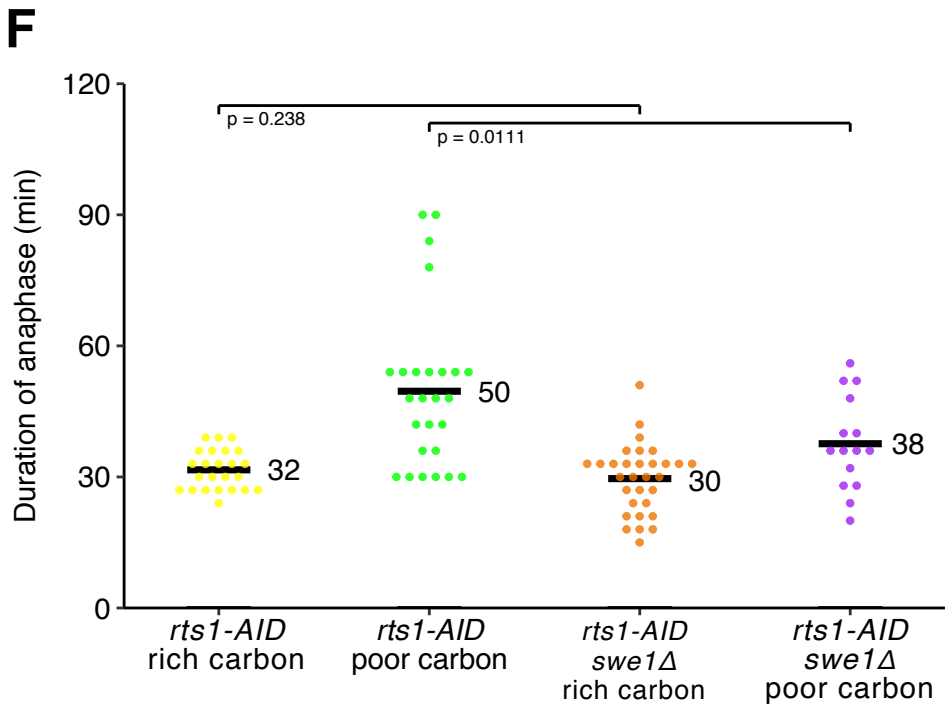

Figure S5

Dot plot versions of the data used to generate Figures 11C,D